THE EFFECT OF MIXING, RADIATION, AND FINITE-RATE COMBUSTION UPON THE FLOW FIELD AND SURROUNDINGS OF THE EXHAUST PLUMES OF ROCKET ENGINES BURNING RP1 (KEROSENE) AND LIQUID OXYGEN

GASL TECHNICAL REPORT NO. 681

O. Fortune and R. Edelman

N68-15848 (ACCESSION NUMBER)

93 (PAGES)

CR-61494 (NASA CR OR TMX OR AD NUMBER)

(THRU) 1

(CODE) 33

(CATEGORY)

FACILITY FORM 602

GENERAL APPLIED SCIENCE LABORATORIES, INC.

MERRICK AND STEWART AVENUES, WESTBURY, L.I. NEW YORK 11590 • 516-333-6960

cy #16

THE EFFECT OF MIXING, RADIATION, AND FINITE-RATE COMBUSTION UPON THE FLOW FIELD AND SURROUNDINGS OF THE EXHAUST PLUMES OF ROCKET ENGINES BURNING RP1 (KEROSENE) AND LIQUID OXYGEN

GASL TECHNICAL REPORT NO. 681

O. Fortune and R. Edelman

Prepared Under Contract # NAS8-21047

Prepared for

National Aeronautics and Space Administration
George C. Marshall Space Center
Huntsville, Alabama

Prepared by

General Applied Science Laboratories, Inc.
Wholly Owned Subsidiary of The Marquardt Corp.
Merrick and Stewart Avenues
Westbury, L.I., New York

L. M. Nucci

L. M. Nucci
President

December 1967

ACKNOWLEDGEMENTS

The authors wish to acknowledge the work done by Messrs. Jack Melnick and Harold Schechter in programming the radiation analysis of Reference 2, and the many endeavors of Mr. Albert Petraglia in the development of the soot combustion quasi-global chemistry model.

ABSTRACT

A free shear layer mixing analysis, a "quasi-global" finite rate oxidation model for hydrocarbon burning, and a carbon cloud radiation analysis are herein coupled in an attempt to describe the turbulent exhaust plume of a hydrocarbon-oxygen rocket engine.

The free shear layer mixing analysis is based on the boundary layer equations.

The development of the "quasi-global" chemistry model is presented and comparison is made with experiments.

The radiation analysis employs the grey gas assumption, takes into account the affects of plume curvature, and includes the back radiation to the engine base.

TABLE OF CONTENTS

LIST OF FIGURES

NOMENCLATURE

a	parameter defined in Eq. (14).
B	black body intensity (BTU/sec-ft^2-solid angle)
C_p	specific heat at constant pressure (BTU/lbm)
E_i	ith incomplete gamma function
h	static enthalpy (BTU/lbm)
H	total enthalpy (BTU/lbm)
I	plume radiation intensity (BTU/sec-ft^2-solid angle)
Le	Lewis number
M	Mach Number
n	distance in the direction normal to the plume boundary streamline (ft.)
Pr	Prandtl number
p	pressure (lbf/ft^2 or atmospheres)
q	heat transfer flux (BTU/sec-ft^2)
r	radial location of an engine base point (ft.)
R_c	local radius of curvature (ft.)
$\tilde{R}$	Universal gas constant: 1.986 cal/^{o}K-gm-mole
s	distance along the plume boundary streamline (ft)
Sc	Schmidt number
t	time (seconds)
t	thickness of plume radiating layer (ft.)
T	temperature (^{o}K)
u	velocity component in the s direction (ft/sec)
v	velocity component in the n direction (ft/sec)
W	molecular weight
$\dot{w}$	mass rate of species production (1/second)
x	distance in the axial direction (ft/sec)
y	distance in the direction normal to the axis (ft/sec)
α	mass fraction
$\tilde{\alpha}$	element mass fraction
$\cos\beta$	direction cosine of I with respect to the n direction
δ^*	displacement thickness (ft)
$\cos\theta$	direction cosine of I with respect to a normal from the engine base
$\varkappa$	average absorption coefficient
μ	turbulent eddy viscosity coefficient (lbf-sec/ft^2)
ρ	density (slugs/sec)
σ	Stefan-Boltzman constant: 4.99×10^{-12} BTU/sec-ft^2-(^{o}K)^4
φ	local inclination of plume to axial centerline
ψ	stream function defined in Eqs. (5) & (6)
Ψ	net asimuthal angle between a point on the base and a point on the plume surface
Ω	plume radiation solid angle

Subscripts

l	lowest grid point in stream function mesh
B	engine base
c	solid carbon
e	outer edge of plume mixing region
F	fuel
M	highest grid point in stream function mesh
m,n	ψ and s index, respectively, in finite difference grid
PB	plume boundary streamline
r	radiation

Superscripts

i	ith chemical specie

SECTION A

PLUME FLOW FIELD

TECHNICAL REPORT # 681

THE EFFECT OF MIXING, RADIATION, AND FINITE-RATE COMBUSTION UPON THE FLOW FIELD AND SURROUNDINGS OF THE EXHAUST PLUMES OF ROCKET ENGINES BURNING RP1 (KEROSENE) AND LIQUID OXYGEN

O. Fortune and R. Edelman

I. INTRODUCTION

Previous work on exhaust plume afterburning effects, Refs. 1 and 2, established (1) a free shear layer mixing analysis for fully expanded nozzle flows, (2) a "quasi-global" finite rate oxidation mechanism for high molecular weight hydrocarbons,and (3) a free shear layer carbon cloud radiation analysis. The free shear layer mixing analysis is based on the solution of the boundary layer equations and makes use of the best available formulations for eddy transport coefficients. The "quasi-global" oxidation mechanism involved eight active species entering into nine elementary reactions coupled to a global reaction involving the partial oxidation of the high molecular weight hydrocarbon molecule. Thus, a total of nine active (N_2 inert) and ten reactions were considered. The radiation analysis includes the affect of radiation on the flow field as well as the back radiation to the vehicle base. The grey gas assumption is made and the ffects of curvature are included.

In the present study the finite rate "quasi-global" chemistry of Ref. 1 has been improved, coupled to the radiation analysis of Ref. 2, and set in a flow field specially designed for the under-expanded plume radiation problem. In addition, an attempt has been made, based on experimental results, to formulate a quasi-global finite rate chemistry model for the burning of the very small carbon particles that are dispersed throughout the plume.

II. PLUME FLOW FIELD GOVERNING EQUATIONS

In the F-1 engine, which is typical of rocket engines burning hydrocarbon fuels and liquid oxygen, the plume exhaust gases are in general fuel rich, which means that small carbon particles (with a mean diameter of 300 to 500 A^{o}) are dispersed throughout the rich region. Furthermore, the temperature of the exhaust gases remains high enough (near 2000^{o}K) so that it is quite possible for the upper layers of the plume to mix and burn with the surrounding air in a short enough period of time so that there are radiating soot particles at over 2000^{o}K within a few nozzle exit diameters of the base and nozzle exit, even though the plume is definitely supersonic, or even hypersonic.

In the F-1 engine this affect will be enhanced by the fuel rich auxiliary engine turbine exhaust gases that are dumped into the nozzle boundary layer region, as shown in Figure 1, and are thus the first to mix with the surrounding air, and at a lower velocity than the main flow.

Thus it is important to analyze the amount of radiant heat transfer that will be generated from the solid carbon to see if it will cause a significant rise in temperature on the base of the engine, or adjacent nozzle surfaces.

Since this study is limited to radiation from the carbon, which is significant only in the shear layer, it is assumed that the inner boundary of this layer is adiabatic. Further, it is also assumed that within the plume, radiation components parallel to the plume boundary streamline are negligible compared to the components normal to the boundary. Using curvilinear coordinates, s is the arc distance along the boundary and n the normal to the streamline. By definition $n = 0$ on the plume boundary streamline. The carbon particle cloud is considered as a continuum in dynamic and thermal equilibrium with the gas phase, and for a free shear layer, which

is thin compared to the plume, the parabolic boundary layer equations that shall be used to describe the mixing in the plume ambient air interface are exactly the same as those for a steady axisymmetric boundary layer on a blunt, curved body (cf. Ref. 4):

Continuity:

$$\frac{\partial(\rho u y)}{\partial s} + \frac{\partial(\rho v y)}{\partial n} = 0 \tag{1}$$

Momentum:

$$\rho u \frac{\partial u}{\partial s} + \rho v \frac{\partial u}{\partial n} = - \frac{dp}{ds} + \frac{\partial}{\partial n} \left(\mu \frac{\partial u}{\partial n} \right) \tag{2}$$

Energy:

$$C_p \rho u \frac{\partial T}{\partial s} + C_p \rho v \frac{\partial T}{\partial n} = u \frac{dp}{ds} + \mu \left(\frac{\partial u}{\partial n}\right)^2 - \rho \sum_{i=1}^{k} h^i \dot{w}^i$$

$$+ \frac{\mu}{Sc} \frac{\partial T}{\partial n} \sum_{i=1}^{k} c_p^i \frac{\partial \alpha^i}{\partial n} - \frac{\partial q_r}{\partial n} \tag{3}$$

where q_r is the radiation heat flux.

Diffusion:

$$\rho u \frac{\partial \alpha^i}{\partial s} + \rho v \frac{\partial \alpha^i}{\partial n} = \frac{\partial}{\partial n} \left(\frac{\mu}{Sc} \frac{\partial \alpha^i}{\partial n} \right) + \rho \dot{w}^i \tag{4}$$

where $y = y(s)$ is the radius of the dividing streamline.

The von Mises transformation is used to relate the (s,n) and (s,ψ) coordinate systems, where the stream function ψ is defined by

$$\frac{\partial \psi}{\partial n} = \rho u y \tag{5}$$

and

$$\frac{\partial \psi}{\partial s} = - \rho v y \tag{6}$$

Thus if $b = b\ (s, \psi)$

$$\frac{\partial b}{\partial s})_n = \frac{\partial b}{\partial s})_\psi + \frac{\partial b}{\partial \psi})_s \frac{\partial \psi}{\partial s} = \frac{\partial b}{\partial s})_\psi - \rho v y \frac{\partial b}{\partial \psi})_s \tag{7}$$

$$\frac{\partial b}{\partial n})_s = \frac{\partial b}{\partial \psi})_s \frac{\partial \psi}{\partial n} = \frac{\partial b}{\partial \psi})_s \rho u y \tag{8}$$

Since $\frac{\partial y(s)}{\partial n} = 0$, it can easily be shown that the stream function identically satisfies the continuity equation.

In addition, the equation of state is

$$p = p(\rho, W, T) \tag{9}$$

It should be noted that the molecular weight of the mixture is calculated including the contribution of the mass fraction of solid carbon, if any. The mixture density is

$$\rho = \frac{p}{\tilde{R} T \sum_{i=1}^{12} \frac{\alpha^i}{W^i}} \tag{10}$$

where graphite is the thirteenth and last chemical specie.

Using the stream function, the conservation equations may now be written

Momentum:

$$\frac{\partial u}{\partial s} = - \frac{1}{\rho u} \frac{dp}{ds} + \frac{\partial}{\partial \psi} \left(a \frac{\partial u}{\partial \psi} \right) \tag{11}$$

Energy:

$$C_p \frac{\partial T}{\partial s} = \frac{1}{\rho} \frac{dp}{ds} + \frac{\partial}{\partial \psi} \left(\frac{aC_p}{Pr} \frac{\partial T}{\partial \psi} \right) - \frac{1}{u} \sum_{i=1}^{k} h^i \dot{w}^i \tag{12}$$

$$+ a\left[\left(\frac{\partial u}{\partial \psi}\right)^2 + \frac{1}{Sc} \frac{\partial T}{\partial \psi} \sum_{i=1}^{k} C_p^i \frac{\partial \alpha^i}{\partial \psi}\right] - y \frac{\partial q_r}{\partial \psi}$$

Diffusion:

$$\frac{\partial \alpha^i}{\partial s} = \frac{\partial}{\partial \psi} \left(\frac{a}{Sc} \frac{\partial \alpha^i}{\partial \psi} \right) + \frac{\dot{w}^i}{u} \tag{13}$$

where

$$a \equiv \rho u \mu y^2 \tag{14}$$

Consider the flow field to be divided up into a grid in (s, ψ) coordinates, with $\psi = \psi_p$ on the s axis. Let ψ_M be the top grid point, and ψ_1 the bottom grid point. In general, $\psi_1 > 0$.

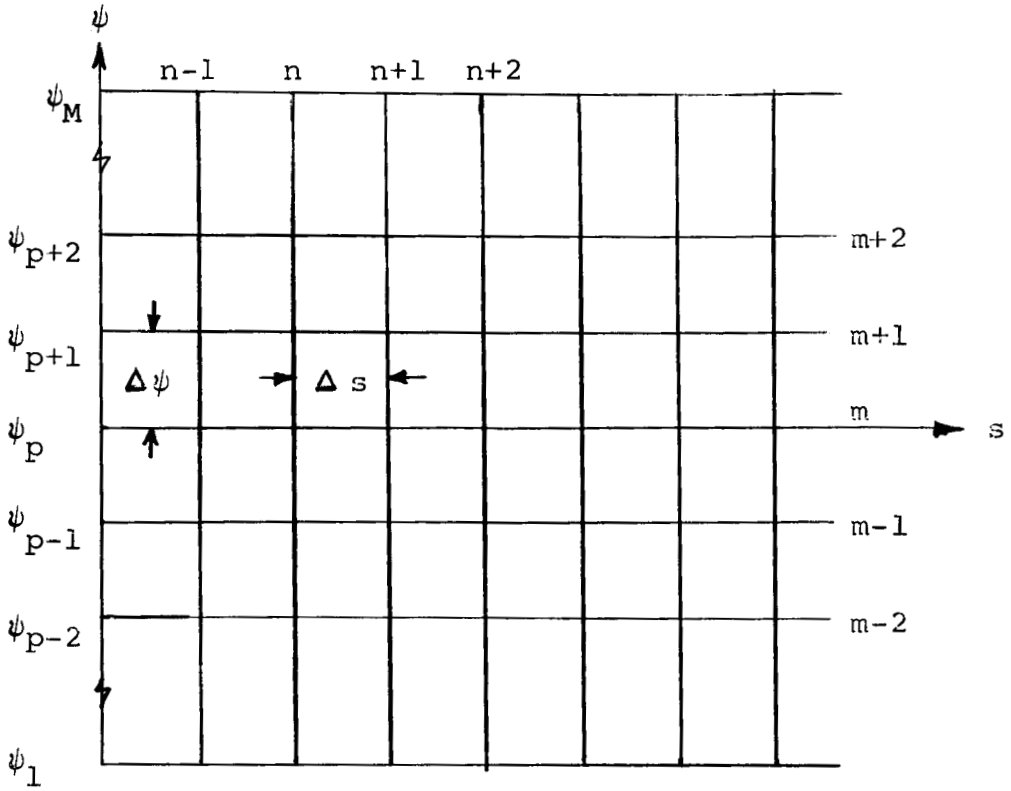

Since the conservation equations are in the form of parabolic differential equations they may be written using the following explicit finite difference scheme where the derivatives of an arbitrary independent variable, F, are evaluated by

$$\left(\frac{\partial F}{\partial s}\right)_{n+1,m} = \frac{F_{n+1,m} - F_{n,m}}{\Delta s} \tag{15}$$

$$\left(\frac{\partial F}{\partial \psi}\right)_{n,m} = \frac{F_{n,m+1} - F_{n,m-1}}{2\Delta \psi} \tag{16}$$

$$\left[\frac{\partial}{\partial\psi}\left(a\,\frac{\partial F}{\partial\psi}\right)\right]_{n,m}=\frac{a_{n,m+\frac{1}{2}}(F_{n,m+1}-F_{n,m})-a_{n,m-\frac{1}{2}}(F_{n,m}-F_{n,m-1})}{(\Delta\psi)^2} \tag{17}$$

where

$$a_{n,m\pm\frac{1}{2}}=\frac{a_{n,m}+a_{n,m\pm1}}{2} \tag{18}$$

Using these relations, the conservation equations become

Momentum:

$$u_{n+1,m}=u_{n,m}-\frac{\Delta s}{(\rho u)_{n,m}}\left(\frac{dp}{ds}\right)_{n+1}$$

$$+\frac{\Delta s}{(\Delta\psi)^2}\left[a_{n,m+\frac{1}{2}}(u_{n,m+1}-u_{n,m})+a_{n,m-\frac{1}{2}}(u_{n,m-1}-u_{n,m})\right] \tag{19}$$

Energy:

$$T_{n+1,m}=T_{n,m}+\frac{\Delta s}{(\rho u)_{n,m}}\left(\frac{dp}{ds}\right)_{n+1}-\frac{\Delta s}{(uC_p)_{n,m}}\sum_{i=1}^{k}(h^i\dot{w}^i)_{n,m}$$

$$+\left(\frac{a}{C_p}\right)_{n,m}\frac{\Delta s}{4(\Delta\psi)^2}(u_{n,m+1}-u_{n,m-1})^2-\Delta s\left(\frac{\gamma}{C_p}\,\frac{\partial q_r}{\partial\psi}\right)_{n,m}$$

$$+\frac{\Delta s}{C_{p_{n,m}}}\,\frac{1}{(\Delta\psi)^2}\left\{\left(\frac{aC_p}{Pr}\right)_{n,m+\frac{1}{2}}(T_{n,m+1}-T_{n,m})+\left(\frac{aC_p}{Pr}\right)_{n,m-\frac{1}{2}}(T_{n,m-1}-T_{n,m})\right. \tag{20}$$

$$\left.+\tfrac{1}{4}\left(\frac{a}{Sc}\right)_{n,m}\sum_{i=1}^{k}(T_{n,m+1}-T_{n,m-1})\,C^i_{p_{n,m}}\,(\alpha^i_{n,m+1}-\alpha^i_{n,m-1})\right\}$$

The derivation of $\frac{\partial q_r}{\partial\psi}$ is explained in Section B of this report.

Diffusion:

$$\alpha^{i}_{n+1,m} = \alpha^{i}_{n,m} + \Delta s \left(\frac{\dot{w}^{i}}{u} \right)_{n,m} + \frac{\Delta s}{(\Delta\psi)^2} \left[\left(\frac{a}{Sc} \right)_{n,m+\frac{1}{2}} (\alpha^{i}_{n,m+1} - \alpha^{i}_{n,m}) + \left(\frac{a}{Sc} \right)_{n,m-\frac{1}{2}} (\alpha^{i}_{n,m-1} - \alpha^{i}_{n,m}) \right] \tag{21}$$

Thus, the calculation marches forward in steps of Δs solving for $F_{n+1,m}$ in terms of $F_{n,m-1}, F_{n,m}, F_{n,m+1}$, etc. Δs must be kept small for the solution to be stable. This is done by use of the following criteria:

(1) For $\psi_2 \leq \psi \leq \psi_M$

$$\Delta s_1 = \frac{(\Delta\psi)^2}{3 \left[\left(\frac{a}{Sc}\right)_{n,m+\frac{1}{2}} + \left(\frac{a}{Sc}\right)_{n,m-\frac{1}{2}} \right]}$$

(2) For $\psi = \psi_1$

$$\Delta s_2 = \frac{(\Delta\psi)^2}{6 \left(\frac{\rho u\, Sc}{\mu} \right)_{n,1}}$$

(3) $\Delta s_3 = \text{minimum } (\Delta n_i)$

Then $\Delta s = \text{minimum } (\Delta s_1, \Delta s_2, \Delta s_3)/\text{XMPS}$, where XMPS is an inputted constant.

Grid points are added at both ψ_M and ψ_1 as the plume and ambient air mix. The criterion for adding a grid point is that there be a difference of more than 0.1% in u, T or α^{i}, between ψ_M and ψ_{M-1}, or ψ_2 and ψ_1.

When one less than twice the initial number of grid points are in use alternate points are discarded, and the calculation proceeds using the original number of grid points. This process is repeated throughout the calculation. It does not introduce significant errors, since the u, T, and ρ^i profiles will be smooth by the time the grid is halved, even when the initial profiles had a unit step function difference between the plume and its surroundings.

The initial plume boundary streamline must, of course, be preserved throughout the length of the calculation.

SECTION B

RADIATION ANALYSIS

III. PLUME RADIATION EFFECTS

In Section A the term q_r, the radiant heat flux, was introduced, but not evaluated. The determination of the radiant heat flux, both across the plume, and to the base, is one of the chief objectives of this work. In Reference 2 Slutsky and Melnick presented an analysis for the carbon radiation problem, which shall be summarized below. This radiation analysis has now been coupled to an improved form of the mixing and finite-rate combustion analysis of Reference 1. Also, during the course of this work an attempt was made to formulate a global finite-rate combustion model for the burning of the plume carbon particles.

It appears from the work of References 2 and 5, for example, that for the chemical composition and temperature typical of the F-1 engine plume, that the principal source of radiation is the very small solid carbon particles that are dispersed throughout the fuel rich regions of the plume.

A. Local Plume Radiation Flux

In Reference 2, an analysis was developed which resulted in the following expression for the flux across the radiating layer:

$$q(\xi_i)=2\pi \int_0^1 d(\cos\beta)\left[\int_0^{\xi_i} B(\xi)\, e^{-\left(\frac{\xi_i+\xi}{\cos\beta}\right)} d\xi \right.$$

$$\left. + \int_0^{\xi_i} B(\xi)\, e^{-\left(\frac{\xi_i-\xi}{\cos\beta}\right)} d\xi - \int_{\xi_i}^{\xi_e} B(\xi) e^{-\left(\frac{\xi-\xi_i}{\cos\beta}\right)} d\xi \right] \tag{22}$$

where

$$\xi_i \equiv \int_{n_1}^{n_i} \rho_c \chi dn, \quad \xi_e \equiv \int_{n_1}^{n_e} \rho_c \chi dn, \quad B \equiv \frac{\sigma T^4}{\pi} \tag{23}$$

and

$\cos\beta$ = the direction cosine of the radiation intensity with respect to n, the direction normal to the plume boundary streamline.

Thus,

$$-\frac{\partial q_r(n_i)}{\partial n} = 2\pi\rho_c\chi\left\{-2B(\xi_i)+\int_o^{\xi_e} B(\xi)\ \left[E_1(\xi_i+\xi)+E_1(|\xi_i-\xi|)\right]\,d\xi\right\} \quad (24)$$

where E_1 is the first incomplete gamma function of the form

$$E_n(a) = \int_1^{\infty} e^{-ab}b^{-n}db = \int_o^{1} e^{-\frac{a}{c}}c^{n-2}dc \quad (25)$$

for $c = \frac{1}{b}$

Using the method of parts, and the relation

$$E_2(a) = -\int_{a_1}^{a_2} E_1(a)\ da$$

$\frac{\partial q_r(n_i)}{\partial\psi}$ is readily evaluated numerically at n_i, and by Equation (8) $y\frac{\partial q_r}{\partial\psi}$ is simply $\frac{1}{\rho u}\frac{\partial q_r}{\partial n}$.

B. Radiation to the Base Region

The radiation energy flux from any point Q(x,y) of the plume surface to any point P(o,r) of the base may be very simply expressed as

$$q_r(P) = \int I(\overline{QP})\cos\theta d\Omega \quad (26)$$

where θ is the angle between the vector QP and the normal to the base $\bar{n}_B$, $I(\overline{QP})$ is the intensity of the radiation in the direction $\overline{QP}$, and Ω is the appropriate solid angle for the plume surface (cf. Figure 2).

Now $d\Omega$ may be expressed as

$$d\Omega = \frac{\cos\beta dA}{(\overline{QP})^2} \tag{27}$$

where β is the angle between $\overline{QP}$ and $\bar{n}$, the normal to the plume surface element dA (cf. Fig. 2).

The above may be expressed more explicitely by representing dA as an element on the cone tangent to the plume surface at Q(x,y). As shown in Figures 2, 3 and 4, it is possible using an ijk triad of unit vectors to write $\overline{QP}$, $\bar{n}$, and $\bar{n}_B$ in terms of x,y(x), $\frac{dy}{dx}$, and Ψ:

$$\overline{QP} = \bar{i}x - \bar{j}y\sin\Psi + \bar{k}(r - y\cos\Psi)$$

$$\bar{n} = \bar{i}y\frac{dy}{dx} + \bar{j}y\sin\Psi + \bar{k}y\cos\Psi \tag{28}$$

$$\bar{n}_B = -\bar{i}$$

Here Ψ is the net asimuthal angle of pt. Q(x,y) with respect to pt. P(0,r).

By definition:

$$\cos\beta = \frac{\overline{QP}\cdot\bar{n}}{|QP|\ |n|} \qquad \cos\theta = \frac{\overline{QP}\cdot\bar{n}_B}{|QP|\ |n_B|} \tag{29}$$

Using $\tan\varphi \equiv \frac{dy}{dx}$

$$\cos\beta = \frac{\cos\varphi(x\tan\varphi - y + r\cos\Psi)}{\sqrt{x^2 + y^2 + r^2 - 2yr\cos\Psi}} \tag{30}$$

$$\cos\theta = \frac{x}{\sqrt{x^2 + y^2 + r^2 - 2yr\cos\Psi}} \tag{31}$$

The element surface area on the tangent cone can be expressed as

$$dA = \frac{y}{\cos\varphi}\, d\Psi dx \tag{32}$$

Using the above relations we may substitute in Equation (26) to obtain

$$q(P) = \int_x y(x)xdx \left[\int_\Psi \frac{I(\cos\beta, x)(x\tan\varphi - y + r\cos\Psi)}{(x^2+y^2+r^2-2yr\cos\Psi)^2}\, d\Psi\right] \tag{33}$$

The domain of integration for $\int_\Psi$ can be restricted by considering that we are only interested in cases where the integral is positive. Hence,

$$x\tan\varphi - y + r\cos\Psi \geq 0 \tag{34}$$

is required.

It now remains to evaluate $I(\cos\beta,x)$. It was shown in Ref. 2 that, except for $\cos\beta \approx 0$

$$I(\cos\beta,x) = 2e^{-\left(\frac{\xi_e}{\cos\beta}\right)} \int_0^{\xi_e} B(\xi) \cosh\left(\frac{\xi}{\cos\beta}\right) \frac{d\xi}{\cos\beta} \tag{35}$$

For $\cos\beta \to 0$ it is necessary to take into account the plume surface curvature. As is explained in Ref. 2, Equation (35) is modified to

$$I(\cos\beta,x) = 2\, e^{-\xi_M} \int_0^{\xi_M} B(\xi) \cosh \xi d\xi \tag{36}$$

where

$$\xi_M = \int_0^z \rho_c \varkappa dz$$

and z is obtained for $t \equiv n_e - n$ and $t_M = R_c(1-\sin\beta)$ and by the transformation

$$dz = -\frac{(R_c - t)\, dt}{\sqrt{(R_c\cos\beta)^2 + t(t-2R_c)}} \quad ; \quad t \le t_m \tag{37}$$

as illustrated in Figure 5.

Thus, the final form of the intensity is

$$I(\cos\beta) = 2e^{-\xi_M} \int_0^{t_M} \frac{B(t) \cosh \zeta\rho_c\varkappa\, (R_c - t)}{\sqrt{(R_c\cos\beta)^2 + t(t-2R_c)}}\, dt \tag{38}$$

where

$$\zeta(\cos\beta,t) = \int_t^{t_M} \frac{\rho_c \varkappa (R_c - t)}{\sqrt{(R_c\cos\beta)^2 + t(t-2R_c)}}\, dt \tag{39}$$

and

$$\xi_M=\xi(\cos\beta,0) = \int_o^{t_M} \frac{\rho_c \varkappa (R_c-t)}{\sqrt{(R_c\cos\beta)^2+t(t-2R_c)}} \, dt \qquad (40)$$

The above is used in the evaluation of $q_r(P)$ in Equation (26).

C. Results of Radiant Base Heating Calculations

Appendix B lists the initial conditions and nozzle and plume geometry for two sample plume calculations. The calculations were carried out to a downstream distance of one nozzle exit radius. Figures 6 and 7 show the integrated radiant heat flux to several base radii for these calculations. The conclusion based on these conditions would be that radiant heat transfer does not cause significant base heating within a period of time for which it is reasonable to expect the F-1 engine to be operating, and that convective heat transfer may be the dominant mode of base heat transfer. The calculation could, of course, be carried out to a greater distance.

In evaluating whether plume radiation has a significant heating effect on the engine base it is necessary to consider both how long the engine will be firing, and the history of the magnitude of the radiant flux during the firing period. A maximum firing time of several hundred seconds seems reasonable both for take-offs and in-space maneuvering. In space, the plume will present a far greater total surface area to the base, but the plume gases will have expanded to a temperature less than half of the nozzle exit temperature. If the assumption is accepted that the carbon particles are essentially at the same temperature as the gas surrounding them, then the lower plume temperature will at lease partially compensate for

the large surface area. Similarly, during a launching, as the free stream pressure decreases with altitude, the reduction in plume temperature due to expansion will oppose the affect of increased plume surface area being presented to the base.

Although radiant base heating may not be significant, it would be worthwhile to extend the present calculation to include radiation to bodies such as other F-1 nozzles clustered near the plume. A look at the full radiation analysis in Ref. 2, or the summary presented in this report, will show that this is a relatively simple and straightforward task.

SECTION C

FINITE RATE CHEMISTRY

IV. ATTEMPTED SIMPLIFICATION OF ANALYSIS OF CHINITZ AND BAURER

In Reference 3 Chinitz and Baurer presented a chemical kinetic analysis for the finite rate oxidation of propane with air. Thirty gaseous species (N_2 was considered as a diluent) participated in sixty-nine chemical kinetic reactions in forming a chain of intermediate hydrocarbons between C_3H_8 and equilibrium products such as CO, CO_2, H_2O, etc., as is shown in Figure 8. One of the suggestions for future work in Reference 1 was to see if this reaction chain could be simplified sufficiently to make it economically feasible from the point of view of computer running time in a mixing calculation on an IBM 7094. Upon investigation it was found that the elimination of just a few of the species (and their associated reactions) that were present only as traces during the preignition period very significantly effected both the preignition and reaction times. When major deletions were made, the results were completely distorted and worthless.

The conclusion is that the analysis of Chinitz and Baurer cannot be further simplified in order to reduce the computer solution time. Hence, it was concluded that at present the "quasi-global" chemistry model remains the only practical hydrocarbon finite rate chemistry scheme for the description of multi-dimensional flow fields.

V. IMPROVEMENT OF THE PARAFFIN FINITE RATE OXIDATION QUASI-GLOBAL COMBUSTION MODEL

In Reference 1 a "quasi-global" finite rate chemistry model for paraffin oxidation was developed using the analysis of Chinitz and Baurer as a guide. The final form of the model (system III) was

$$C_nH_{2n+2} + \frac{n}{2} O_2 \longrightarrow nCO + (n+1) H_2$$

where

$$-\frac{dY_F}{dt} = \frac{10^{13}}{(P)^{.825}} \left[\frac{.9T_i}{1000} - .5\right] Y_F^{\frac{1}{2}} Y_{O_2} e^{-13,740/RT}$$

Here Y denotes molar concentration (moles/cm^3) and P is in atmospheres.

It was suggested in Reference 1 that the representation of the preignition period might be improved by the addition of the five chemical kinetic reactions presented in Reference 3 for formaldehyde (HCHO) and formyl (CHO), and to formulate the quasi-global reaction between HCHO and the paraffin. CHO and HCHO were added to the chemical kinetic system of reaction equations - which are listed in full in Appendix C - and a great variety of quasi-global models were investigated. It was found that for the preignition period, the quasi-global reaction betweeen the paraffin and CHO, rather than HCHO, should be used. The probable explanation for this is that HCHO has a far more exothermic heat of

formation than CHO and this will cause a larger temperature rise during its formation. Furthermore, it was found that it was not possible to write a reaction of the form

$$C_nH_{2n+2} + \frac{n}{2} O_2 \longrightarrow n\ CHO + \frac{n+2}{2} H_2$$

but rather that CO or CO_2 must also be formed by the quasi-global model in order to obtain a realistic ignition delay time and reaction time. Also, it was finally concluded that the best representation would form CO for "high" temperatures, and CO_2 for "low" temperatures. It was found that for initial mixture temperatures above $1300^{\circ}K$ a model using CO was best. When the initial temperature was less than $1300^{\circ}K$ a CO_2 model was used. However, during the reaction period it is of course necessary to change from the CO_2 model to the CO model. This switchover temperature was determined to be not $1300^{\circ}K$, but $1500^{\circ}K$ (unless the sum of the mass fractions of CO and CO_2 was greater than 10%, which means that the combustion process is near completion). This variation in cutoff temperature is associated with the fact that unless the burning process is well into the reaction period, the forming of CO instead of the more exothermic CO_2 acts as a damper upon the combustion process for temperatures below $1500^{\circ}K$. This manipulation of the

boundary temperature between the two quasi-global models may seem to be a bit of unnecessary fussiness. However, it is important because, as will be discussed in detail later, the paraffin combustion process is apparently extremely sensitive to temperature. Also, in flow field calculations with significant turbulent mixing, there is far less of a smooth history of combustion on each streamline than there is for a one-dimensional calculation. Thus, it is important to have as realistic a model as possible for local temperatures between 1300 and 1500°K.

The question of the rate of formation of CO and CO_2 in the burning of hydrocarbons and graphite has received a good deal of attention (cf. Refs. 6 to 21). Unfortunately, the various theories and experiments are contradictory. It is clear that CO is present during the burning process in a higher concentration than at equilibrium, and plays an important role with regards to the ignition and reaction times. As is true with many questions for hydrocarbon combustion, more experimental results are needed. The final quasi-global model (system IV) is

$$C_nH_{2n+2} + \frac{n}{2}\left(1 + \frac{k}{2}\right) O_2 \longrightarrow \frac{n}{2} CHO + \left(\frac{3n}{4} + 1\right) H_2 + \frac{n}{2}\left(kCO_2 + (1-k)\, CO\right) \tag{41a}$$

where

$$k = \begin{cases} 0; \text{ "high" temperature zone} \\ 1; \text{ "low" temperature zone} \end{cases}$$

and

$$-\frac{dY_F}{dt} = K \left(1.9 - \frac{.54T}{1000}\right) P^{\frac{1}{2}} Y_F^{\frac{1}{2}} Y_{O_2} e^{-13,740/RT} \qquad (41b)$$

where

$$K = \begin{cases} 3 \times 10^8 ; & \text{"high" temperature zone} \\ \dfrac{3 \times 10^8 W_{CO}}{W_{CO_2}} = 1.91 \times 10^8 ; & \text{"low" temperature zone} \end{cases}$$

It may be noted here that the philosophy that has been developed towards formulating quasi-global models is that one can expect to arrive at the form

$$-\frac{dY_F}{dt} = kf(T) P^{\alpha} Y_F^{\beta} Y_{O_2}^{\gamma} e^{-E/RT} \qquad (42)$$

and that k, f(T), and α will vary strongly as a function of what the products of the quasi-global model are, and of the intermediate species included in the elementary reactions of the chemical kinetic system.

A look at the rate equation for the present global model shows that it will fail at 3520°K. Since it is impossible for a paraffin to exist at this high a temperature, this is not a cause for concern.

In Figures 9 through 11 systems III and IV are compared with the analysis of Chinitz and Baurer over a range of temperatures and pressures. It is clear that system IV is superior to system III and provides an excellent approximation to the detailed kinetic analysis.

System IV does not (and cannot) exhibit the peak temperature CO_2 overshoot of the kinetic analysis. Since it is not yet known whether this oversoot occurs physically, this is an excusible omission. System IV in general does a better job of simulating the ignition delay period than system III. However, it is not possible to construct, using only a few intermediate species, a quasi-global system that will not exhibit some temperature rise during the pre-ignition period. It is considered satisfactory that system IV matches the behavior of the detailed kinetic system during the reaction period.

A. Comparison With Experimental Results

Although the amount of experimental results available for the finite rate combustion of paraffins is limited, there is enough available to make it possible to compare some aspects of system IV and the analysis of Chinitz and Baurer, with experiment.

The data consists of three types: 1) shock tube experiment reported in References 22 and 23; 2) steady flow spontaneous ignition quenching tube data from References 24, 25, and 26, and 3) model F-1 engine tests reported in Reference 27.

1) Steady Flow Ignition Tube Apparatus

The apparatus of Burwell and Olsen was basically a 16 ft., 1 inch ID stainless steel tube. It was radiantly heated by a 2 inch ID outer concentric tube. Both fuel and air were preheated and then mixed at the tube entrance. Temperature measurements and chemical samples could be taken along the length of the tube. Chemical quenching was provided at the exit by a movable male cylinder which formed an annulus with the female ignition tube. The basic procedure was to establish steady flow with the quenching rod near the entrance of the ignition tube, and then very slowly withdraw the quencher (and thus increasing the system residence time) until ignition occurred, upon which the system was shut-down. An alternate procedure was to leave the position of the quencher constant and begin with a very lean mixture, and then gradually increase the fuel-air ratio.

The fuel was isooctane, and spectrometric and chromatograph analyses were made of preignition samples. Ignition delay results are shown plotted in Figure 12 and will be discussed below with the shock tube data.

Burwell and Olsen found that under certain conditions (increasing fuel richness) there was a temperature rise of as much as 280°K (for an initial temperature of 880°K) during the preignition period, and that as much as 50% of the isooctane decomposed into lower order hydrocarbons before ignition occurred. While these values seem very high, and cause questions to be raised about whether the ignition tube was completely adiabatic, they do indicate that hydrocarbon ignition may be preceded by a preignition period in which there is a substantial rise in temperature - between 10 and 20% of the initial temperature - followed by a much shorter period with an abrupt rise to the equilibrium temperature. This is the type of result that is predicted by system IV, and thus provides another reason for the acceptance of the quasi-global concept.

One explanation for this surprisingly large "preignition" temperature rise is that a higher order paraffin such as isooctane is degraded in a much more complex manner than propane and forms more intermediate products which potentially can liberate thermal energy. It would be of great interest to see experimentally if lower order paraffins such as propane exhibited so great a temperature rise during the preignition period.

Rifkin in commenting upon the work of Burwell and Olsen, Reference 24, presented the results of Salooja, Reference 25, and Rifkin and Walcutt, Reference 26, which are shown in Figure 13. He attributed the longer ignition delay times of Burwell and Olsen, compared to Salooja, to the fact that the quartz steady flow apparatus of Salooja had a larger surface catalytic effect than the stainless steel surface of Burwell and Olsen's apparatus. It should also be noted that if the preignition period were to be defined in the usual manner as the time required to obtain a five per cent rise in initial temperature, the ignition delay times of Burwell and Olsen would be reduced by a factor of two or three, which would bring them closer to other experimental observations.

2) Shock Tube Experiments

Over the course of several years, Nixon, et. al. (Ref. 23), performed a large number of shock tube ignition delay experiments for several hydrocarbons including propane and octane. The hydrocarbon-oxygen mixtures were diluted by from 80 to 99% argon.

A great deal of useful material is contained in these reports. Information on the ignition of propane-oxygen and n-octane-oxygen systems is presented for initial temperatures of

from 900 to 1300°K, pressures from 0.6 to 1.9 atmospheres, and stoichiometric ratios from 0.1 to 1.0. The ignition delay times are shown in Figures 14 and 15 for propane, and octane and dodecane. A comparison of the two figures will show that the ignition delay times are essentially the same for propane and octane, thus validating the assumption that our quasi-global model, based on a propane analysis is useful for the description of kerosene combustion. Furthermore, Figure 16 shows that there is little difference in the ignition delay times of different types of octane.

It is regrettable, however, that most of the shock tube experiments were performed with concentrations of 95 and 99% of argon diluent, for fear of shock tube detonation. Chinitz and Baurer in Reference 3 have previously pointed out that it is not completely realistic to substitute monatomic argon for diatomic nitrogen as a diluent, because, in addition to having a different molecular weight and specific heat capacity, the monatomic molecule will behave differently from the diatomic molecule in participating as a third body in the many elementary chemical kinetic reactions which occur during the burning of the paraffin. Furthermore, when the degree of dilution is so extreme that the total combustion temperature rise is at most a few per cent of the initial temperature, it is not felt that great worth can be attached to the data,

regardless of the nature of the diluent. Indeed, Hawthorne and Nixon in Reference 29 reported the degree to which increasing dilution retarded ignition delay, as shown in Figure 17 for a propane-oxygen-argon misture.

The criterion adopted towards the use of the data of Reference 23 was to use the results of 80% argon dilution tests wherever possible, and 90% argon data where 80% was not available. This means confining ourselves to stoichiometric and lean data. A comparison of ignition delay times for the quasi-global model and the Chinitz-Baurer model is made with the Shell, and Convair data of Reference 22, for propane mixtures at approximately 1 atm. on Figures 18 and 19. In general, the agreement is quite good.

3) Comparison of Steady Flow Data and Shock Tube Data

Ignition delay data for stoichiometric isooctane-air and isooctane-oxygen-argon systems are presented on Figure 20. There is clearly a sharp break between the Shell shock tube data at 1 atm., and the data of Salooja, and Burwell and Olsen at 1 and 1.47 atms., respectively. For the shock tube and steady flow system data to be consistent there would have to be a very rapid change in the ignition delay period between 900 and 1000^{o}K, as would be indicated by path A. Only further experiments with the shock tube at lower temperatures, or the steady flow system at

higher temperatures can resolve whether the two types of experiments yield consistent results. Fortunately, ignition delay times of greater than 1×10^{-2} seconds are not of great interest for this plume analysis since the flow field velocities will typically be at least several thousand feet per second, and hence a particle would be a minimum of several diameters downstream of the exit lip before .01 seconds have elapsed. It may also be noted that the reaction rates for some of the elementary kinetic reactions are not applicable below $800^{\circ}K$ to $1000^{\circ}K$, and that in this low temperature region other kinetic reactions may be required and should be added to the ones used in the quasi-global model and in Reference 3.

B. Comparison of Plume Calculations with Available Experiments

There is still a paucity of experimental data involving measurements of the temperature and chemical concentrations in the F-1 engine plume. Reference 27 reports experimental results that were obtained from static test firings of (a) an F-1 engine (b) a scale model F-1 engine and (c) various small auxiliary rocket engines. Chemical samples could be taken at only one position in the flow field during each test. A spectral radiometer, a photographic pyrometer, and a spectrograph were used to measure radiation from the plume, and thus calculate a temperature map of the plume.

Due to the fact that a structurally strong single-position sampling probe had to be used, the amount of data presented in Reference 27 is by no means comprehensive, since each run provided only one data point as far as chemical composition was concerned. In making use of the experimental data to provide initial conditions for plume calculations, it was decided to average the chemical compositions of the actual F-1 nozzle tests (Runs 74, 76 and 103) and use them as typical of the boundary layer and turbine exhaust gas region, since the probe made a maximum penetration of only .06 r_e into the flow field at the exit plane. Run 30 from the scale model F-1 tests was used to provide the composition of the bulk of the nozzle exhaust. In both cases the values of trace species were taken as that given by the equilibrium calculations presented in Reference 33. The initial values of T, u and mass fractions for the F-1 plume calculation are tabulated in Appendix B. It should be noted that (a) experimentally the intermediate species only amounted to a few percent in the main exhaust flow (b) that the solid carbon mass fraction was less than .02 even in the turbine exhaust region, and (c) that all of the RP1 had been burned or cracked before the exit plane. The intermediate species detected in the flow field were lumped together and considered to be HCHO.

If the concentration of intermediates had been larger and if they had been heavier, higher order hydrocarbons, it would have been more appropriate to represent them as C_9H_{20}. Figures 48 and 49 of Reference 27 present temperature maps made from radiation measurements of 3100 and 4400^{o}A wavelengths, from F-1 model engine runs 168 and 36, respectively. The 3100^{o}A temperature map has an initial temperature of about 2250^{o}K, and shows little change in a distance of one radius from the nozzle exit. The 4400^{o}A map begins with a temperature of 1850^{o}K and reaches 1900^{o}K at one radius, but is rapidly rising at this point. These results may be compared with the case A isotherm map shown in Figure 21, where case A is a sea level calculation with finite rate chemistry. The numerical calculation shows a more rapid rise in temperature, but it is necessary to run the calculation out to a greater distance to be able to fully compare it with the F-1 model engine test results.

The conclusions that the authors of Reference 27 come to regarding the history of carbon formation and burning in the plume are interesting. However, the fact that they are based on many radiation measurements, but relatively few chemical samples, makes it hard to evaluate how well founded these conclusions are. Admittedly, it would be quite expensive to accumulate a large number

of chemical sample data points even using the scale F-1 engine configurations. However, this merely indicates the need of more analytic and basic experimental work for the plume problem rather than specifically hardware oriented tests.

VI. OXIDATION PROCESS FOR CARBON PARTICLES

Since in this analysis it is assumed that the carbon particles in the plume are the source of the radiant energy reaching the base it would be of the greatest interest to be able to predict the rate at which the carbon particles (soot) are formed in the fuel rich layers of the flow field, and the rate at which they are burned off in the leaner regions.

The graphite combustion process has been investigated experimentally and analytically for at least forty years, but there is almost a complete lack of quantitative experiments or theory that is applicable to the description of the formation process and combustion process of carbon particles with a mean diameter as small as 300 to 500^{o}A. Most of the experimental and analytical work that has been performed has dealt with either carbon spheres with diameters of the order of one centimeter, or else ablative surfaces (cf. Refs. 6 to 18). In either case there is a laminar diffusion layer about the particle, or surface, which, according to Scala (cf. Refs. 7 to 10), dominates the oxidation process throughout most of the temperature range that is of interest to us. However, for particles 4×10^{-8}m. in diameter, this diffusive layer is most definitely not the rate controlling factor, and hence

the above analyses and experiments are of little use to us.

Some qualitative work has been done in formulating theories to analyze the soot formation process in fuel rich hydrocarbon flames. Tesner (cf. Refs. 19 and 20) and Homann (Ref. 21) have summarized and correlated much of the work that has been done in the U.S.S.R., Europe, and the U.S.A. on the process of soot formation in hydrocarbon flames, but neither author was able to advance a theory for predicting the rate at which soot formation would occur. Indeed, it is not clear whether the dominant mode of soot formation is through a kinetic chain process where progressively heavier and heavier hydrocarbon polymers, which become more and more unsaturated, are formed until they join in aggregates of thousands of "molecules", each containing hundreds of atoms, which are almost all carbon, or whether carbon atoms are "freed" in simple reactions such as

$$C_nH_m + aO_2 \longrightarrow 2a\ CO + \frac{m}{2} H_2 + (n-2a)\ C \qquad (43)$$

and then form aggregates without further chemical reaction. The former view seems to be supported by the recent experimental work of Echigo, Nishiwake, and Hirata (Ref. 31).

It is quite clear that a great deal more experimental work must be done before any successful quantitative theories for soot formation can be developed.

The finite - rate oxidation process for soot particles already present in hydrocarbon flames also is not well understood. However, Lee, Thring, and Beér (Ref. 32) have performed a set of experiments which make it possible to form a global reaction for the combustion of the carbon particles. This global rate equation should not be thought of as a firmly established analysis, but rather as a useful first estimate which will probably be modified and extended by future experimental work.

The basic experimental apparatus was a laminar diffusion flame inside a quartz tube. The fuel was predominantly propane, with some propylene and ethylene, and was burned with oxygen-enriched, preheated air. Solid and gas samples were taken starting at the axial position at which soot particles were formed in the flow field. The gas samples were analyzed by a chromatographic method, and by an Orsat apparatus. An electron microscope was used in determining the size of the soot particles. A series of runs was made for different overall stoichiometric ratios. Temperatures of from 1200^{o}K to almost 1700^{o}K occurred in the sampling region. The authors were

able to correlate the experimental results for the soot combustion by the relation

$$\frac{d\dot{m}_c}{dt} = \frac{6(1.085) \times 10^4}{\rho_c d_c} \dot{m}_{c_{initial}}^{1/3} \dot{m}_c^{2/3} \frac{pO_2}{\sqrt{T}} e^{-39,300/RT} \quad (44)$$

which is readily transformed to

$$\frac{d\alpha_c}{dt} = .8138 \times 10^{12} \alpha_c \alpha_{O_2} \left(\frac{\alpha_{c_{initial}}}{\alpha_c}\right)^{1/3} \frac{p}{\sqrt{T}} e^{-39,300/RT} \quad (45)$$

by assuming that the soot density ρ_c, is 2 gm/cm^3 and that the mean particle diameter, d_c, is 400°A.

The authors state that they did not detect CO in their sampling. Considering the temperature range of the flow, this is amazing. As far as can be determined from Reference 32, the sampling probe was a simple .5 mm constant diameter stainless steel tube. A standard reference, such as Fristrom and Westenberg (Ref. 30), indicates that a probe must be far more sophisticated in design to chemically freeze the sample. So it appears possible that whatever CO was present in the flow field became CO_2 in the sampling tube as the flow cooled.

Nevertheless, it was decided to tentatively accept the authors' assumption that the soot burning formed CO_2 exclusively. The experimental results of References 27 and 28 indicate that the initial plume carbon mass fractions are low enough so that the amount of CO_2 added to the flow by the soot burning model will not significantly affect the overall plume combustion process. Hence, we shall use the model of Reference 32 as a preliminary analysis in seeing how the soot oxidation process affects the magnitude of the plume radiation.

Equation (45) assumes a one-dimensional flow. To employ it in a multi-dimensional mixing analysis, it is necessary to treat the solid carbon as though it were a separate element whose species are burnt and unburnt carbon. Then $(\alpha_{c_{initial}}/\alpha_c)$ is the ratio of the "element" mass fraction to the unburnt carbon specie mass fraction on each streamline.

The results of using the carbon burning model are compared with the assumption of frozen carbon flow for the data of case A, as shown in Figure 22. It is clear that within one radius downstream of the nozzle exit there has already been significant carbon burning in the hotter poritions of the flow field. And this, of course, will affect the amount of radiation emitted by the plume.

SECTION D

SUMMARY AND RECOMMENDATIONS

VII. SUMMARY AND RECOMMENDATIONS

The coupling of the base radiation analysis to the turbulent mixing program, with hydrocarbon-air finite rate, quasi-global chemistry has shown that plume radiation does not cause significant base heating for a F-1 engine nozzle configuration. It would be of interest to extend the analysis to consider bodies other than a perpendicular base heat shield, such as other nozzles clustered near the plume.

The paraffin-air quasi-global finite rate chemistry analysis of Reference 1 has been improved, particularly with regard to the preignition period. Comparison with shock tube experiments shows that it yields results, at least with respect to ignition times, that are well within an order of magnitude. Also the quasi-global model compares very well (except regarding the CO_2 temperature overshoot) with the more complex and far more time consuming propane-air kinetic chemical model of Chinitz and Baurer. And, of course the quasi-global model can be used to analyse the burning of more complex paraffins than propane, since, as has been shown by the experiments of References 23 and 29, the ignition delay times of the paraffin family vary little with increasing molecular weight.

In order to accurately predict the amount of solid carbon in the plume for the purposes of the radiation analysis, a thorough investigation was made of the experimental and analytical work that has been done on the formation and burning of carbon soot particles in high speed flow. It was found that useful quantitative results were almost completely lacking. However, the work of Lee, Thring, and Beér (Ref. 32) provided a basis for the construction of a tentative global model for the burning of the soot particles.

In general, it may be said that the state of the art with regards to understanding and predicting the presence of solid carbon soot particles in fuel-rich hydrocarbon flames, is at a very low level. It seems clear that the process is not an equilibrium one, since experimental results, such as those presented in References 27 and 28 show solid carbon concentrations an order of magnitude less than the predictions of equilibrium calculations. Hence it is necessary to gather far more experimental data on the problem, and then develop finite-rate chemical models from the experiments. Fortunately, diffusion flame tests should shed light on this problem, and would be relatively inexpensive.

It is also true that more experimental data is needed for hydrocarbon flames in general, for the purpose of evaluating the

various finite-rate chemical mechanisms. The high velocities that the exhaust gases have in the plume require that finite-rate rather than equilibrium chemistry models be used, particularly in the region near the nozzle exit which is the prime source of base radiation. For instance, the experimental results shown in Figure 20 seem to show that there is an extremely rapid increase in ignition delay time as the temperature drops below $1000^{\circ}K$. This could be verified through either more steady flow quenching tube tests, or more shock tube tests. The cost of building a quenching tube rig would not be expensive as experimental facilities go, and even a series of shock tube studies should be less expensive than F-1 engine firings, or possibly even scale model F-1 engine tests.

APPENDIX A

COMPUTER INPUT AND OUTPUT

In Reference 1 the input requirements and output of the computer program for free mixing and system III finite rate chemistry were described in great detail. However, since the flow field has been recast in curvilinear coordinates, and since inputs have been added for the radiation calculation, the preparation of inputs for the computer program will again be discussed in detail.

The program is in Fortran IV (Ibsys 13) language and has been compiled on the IBM 7094 computer. The input format is given below in Table A-I. The turbulent eddy viscosity models are the same as in Reference 1:

Model A: $$\mu = 10^{-4} + \frac{(x + \delta^*_{exit})}{900} \left[(\rho u)_{max} + (\rho u)_{min}\right]$$

Model B: $$\mu = 10^{-4} + \frac{(t_M + \delta^*_{exit})}{900} \left[(\rho u)_{max} - (\rho u)_{min}\right]$$

where the dimensions of μ are lbf-sec/ft^2. ψ_{PB} and $\Delta\psi$ are inputs that must be supplied to the program. It is obviously vital to calculate ψ_{PB} (the plume boundary streamline) correctly, since the entire flow field is constructed about it. From Equation (8)

$$\int_{\psi_a}^{\psi_b} d\psi = y \int_{n_a}^{n_b} \rho u dn \qquad \text{(A-1)}$$

For the F-1 engine, the flow field at the nozzle exit may be thought of as consisting of a central main flow core and an outer boundary layer and turbine exhaust gas region. At the nozzle exit (s=0) y and n coordinates are parallel (before expansion occurs). Hence

$$\psi_{PB} = r_w(\rho u)_{outer} (r_w - r_{core}) + \psi_{core} \qquad \text{(A-2)}$$

$$\psi_{PB} = r_w (\rho u)_{outer} (r_w - r_{core}) + r_w(\rho u)_{core}(r_{core}-0)$$

In general, the outer exhaust gas region will be thinner and have less mass flow than the core region. Hence, initially choose $\Delta\psi$ such that there will be, for instance, ten points in the outer region and two points in the core region and the surrounding air. Thus, the ψ_{PB} grid point would be specified as being the twelfth grid point in this case. As given below in the input format, ψ_{PB}, $\Delta\psi$, and the number of the ψ_{PB} grid point are inputted to specify the setup of the finite difference grid.

The base radiant heat flux will be calculated to as many radial positions on the base as specified. However, since the base radiation calculation is a very time consuming process (of

the same order of magnitude as the finite rate chemistry), the number of radial locations should be kept to a minimum.

This program is not in any way a characteristics program. Hence, the physical coordinates of the plume boundary streamline and the static pressure axial distribution must be found either analytically or experimentally and supplied as inputs to the program. Similarly the change in the physical condition of the nozzle gases as they expand around the exit lip, and the physical state of the free stream air after it passes through the lip shock, must be calculated externally and supplied as inputs to the program.

It may be noted that the radiant base heat flux is negative in the computer output. This has no significance other than that the radiation is in the minus x direction.

TABLE A-I

INPUT FORMAT

Card	Column	Description	Format
1	2-72	Title Card; information inputted here will be printed on every page of output	12A6
2	1-5	Initial number of ψ grid points (M) at starting s.	I5
	6-10	Initial number of grid points at s=0 (must be less than 50)	"
	11-15	= 0 - Finite rate chemistry employed = 1 - Flow is chemically frozen	"
	16-20	= 7 - Viscosity model A used = 8 - " " B "	"
	21-25	Number of grid point at s=0	"
	26-30	MJ; the number of points on base for which radiant heat transfer rate will be calculated. This input may be zero, and must be less than 101.	"
	31-35	= 0 - Mass fractions of solid carbon are chemically frozen = 1 - Solid carbon will burn according to the appropriate global combustion model.	"
3	1-10	Printout interval on plume boundary (Δs) (ft.)	E10.8
	11-20	Maximum axial (x) distance (ft.)-measured from engine base.	"

Card	Column	Description	Format
3	21-30	Starting plume boundary (s) position (ft.)-measured from nozzle exit.	E10.8
	31-40	Starting axial (x) location (ft.) - measured from engine base.	"
4	1-10	Lewis Number	E10.8
	11-20	Prandtl Number	"
	21-30	$\Delta\psi$; distance between grid points (slugs/sec.)	"
	31-40	XMPS; $\Delta s = \Delta s/XMPS$. Usually set equal to 1.	"
	41-50	δ^*_{exit} - boundary layer thickness at nozzle exit (ft.)	"
	51-60	ψ_{PB} - Value of stream function on the plume boundary (slugs/sec.)	"
5	1-10	xp1	"
	11-20	xp2 — End points of domains of pressure polynomials	"
	21-30	xp3	"
	31-40	Blank	"
	41-50	xy1 — End points of domains plume boundary coordinate polynomials	"
	51-60	xy2	"

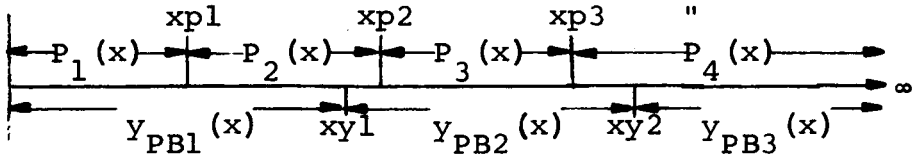

Card	Column		Description	Format
6	1-10	a_1	$P_1(x) = \sum_{j=1}^{6} aj\ (x-x^*)^{j-1}$ $\left(\frac{lbf}{ft^2}\right)$	E10.8
	11-20	a_2	Coefficients of first pressure polynomial.	"
	21-30	a_3		"
	31-40	a_4		"
	41-50	a_5		"
	51-60	a_6		"
	61-70	x^*		"
7	1-70		Second pressure polynomial	7E10.8
8	1-70		Third pressure polynomial	"
9	1-70		Fourth pressure polynomial	"
10	1-70		First plume boundary coordinate polynomial, $y_{PB1}(x) = \sum_{j=1}^{6} bj\ (x-x^*)^{j-1}$ (ft.)	"
11	1-70		Second plume boundary polynomial	"
12	1-70		Third plume boundary polynomial	"

Card	Column		Description	Format
13a	1-10	r_1	Radial locations (ft.) on engine base for which radiant heat transfer flux is calculated. If MJ=0 (Card 2 - CC30) Cards 13i and 14i are completely omitted.	E10.8
	11-20	r_2		"
	- -	--		- -
	60-70	r_7		"
13b	1-10	r_8		"
----------		r_{MJ}		"
14a	1-10	q_1	Values of radiant heat flux (BTU/ft^2sec) at local s. They will, of course, be zero at s=0.	E10.8
	11-20	q_2		"

14b	1-10	q_8		"
----------		q_{MJ}		"
15a	1-10	$T(\psi_1)$	Static temperature (^oK) at each grid point.	E10.8
	11-20	$T(\psi_2)$		"

	61-70	$T(\psi_7)$		"
15b	1-10	$T(\psi_8)$		"

		$T(\psi_M)$		"

Card	Column		Description	Format
16a	1-10	$u(\psi_1)$	Velocity (ft/sec) at each grid point	E10.8
	11-20	$u(\psi_2)$		"

	61-70	$u(\psi_7)$		"
16b	1-10	$u(\psi_8)$		"

		$u(\psi_M)$		"
17A1	1-10	α_H	Species mass fractions at ψ_1. Two cards of mass fractions must be inputted for each grid point. Note that α_{C-F} is only needed when the solid carbon is allowed to participate in the burning process. At s=0, $\alpha_{C-F}=\alpha_C$. For restarts with s>0, α_{C-F} is taken from the output at the end of the previous run.	"
	11-20	α_O		"
	21-30	α_{H_2O}		"
	31-40	α_{H_2}		"
	41-50	α_{O_2}		"
	51-60	α_{OH}		"
	61-70	α_{CO}		"
17B1	1-10	α_{CO_2}		"
	11-20	α_{CHO}		"
	21-30	α_{HCHO}		"
	31-40	$\alpha_{C_9H_{20}}$		"
	41-50	α_{N_2}		"
	51-60	α_C		"
	61-70	α_{C-F}		"

HYDROCARBON-AIR FROZEN CHEMISTRY 2-DIMENSIONAL PLUME

F-1 ENGINE PE/PINF=100 90KF

S= -0. FT X= 1.8066000E 01 FT Y= 5.7900000E 00 FT PHI= -0.0000000E-20 RAD PHI= -0. DEG

PSIA= 2.4583333E-01 S/D= -0. DELSTAR= -1.2745239E 01 DELST-= -3.1139729E 00 DYP/DX= 2.9040000E 00

PRESSURE LEWIS NUMBER PRANDTL NUMBER VISCOSITY STEP NO

3.5400000E 01 1.0000000E 00 1.0000000E 00 1.0000000E-04 0. 1

R BASE= 0. 6.0000000E 00 1.0000000E 01 1.5000000E 01

Q BASE= -0. -0. -0. -0.

PT.	PSI	VELOCITY	TEMPERATURE	VISCOSITY	DENSITY	N(FT.)	MOLEC. WT.	RHO-U	
1	9.2050000E 01	1.4000000E 04	6.0000000E 02	1.0000000E-04	1.3164346-05	-4.5321556 00	1.9917236 01	1.8430076-01	1
2	9.2195000E 01	6.0000000E 03	8.9000000E 02	1.0000000E-04	8.8821226-06	-4.2292566 00	1.9439926 01	5.3292736-02	2
3	9.2340000E 01	6.0000000E 03	8.9000000E 02	1.0000000E-04	8.8821226-06	-3.7593386 00	1.9439926 01	5.3292736-02	3
4	9.2485000E 01	6.0000000E 03	8.9000000E 02	1.0000000E-04	8.8821226-06	-3.2894216 00	1.9439926 01	5.3292736-02	4
5	9.2630000E 01	6.0000000E 03	8.9000000E 02	1.0000000E-04	8.8821226-06	-2.8195046 00	1.9439926 01	5.3292736-02	5
6	9.2775000E 01	6.0000000E 03	8.9000000E 02	1.0000000E-04	8.8821226-06	-2.3495876 00	1.9439926 01	5.3292736-02	6
7	9.2920000E 01	6.0000000E 03	8.9000000E 02	1.0000000E-04	8.8821226-06	-1.8796696 00	1.9439926 01	5.3292736-02	7
8	9.3065000E 01	6.0000000E 03	8.9000000E 02	1.0000000E-04	8.8821226-06	-1.4097526 00	1.9439926 01	5.3292736-02	8
9	9.3210000E 01	6.0000000E 03	8.9000000E 02	1.0000000E-04	8.8821226-06	-9.3983466-01	1.9439926 01	5.3292736-02	9
10	9.3355000E 01	6.0000000E 03	8.9000000E 02	1.0000000E-04	8.8821226-06	-4.6991736-01	1.9439926 01	5.3292736-02	10
11	9.3500000E 01	6.0000000E 03	8.9000000E 02	1.0000000E-04	8.8821226-06	0.	1.9439926 01	5.3292736-02	11
12	9.3645000E 01	1.0000000E 02	2.2400000E 02	1.0000000E-04	5.0931016-05	2.6934986 00	2.8849286 01	5.0931016-03	12

PT.	SPECIFIC HEAT	STATIC H	TOTAL H	SENSE TOT H	GAMMA	MACH NUMBER	TOTAL T	TOTAL P	PT
1	7.057805E-01	-2.314211E 03	1.599869E 03	4.337549E 03	1.341092E 00	7.361793E 00	6.145748E 03	3.324647E 03	1
2	7.989893E-01	-2.285220E 03	-1.566308E 03	1.430013E 03	1.299013E 00	2.600416E 00	1.789778E 03	7.364029E 02	2
3	7.989893E-01	-2.285220E 03	-1.566308E 03	1.430013E 03	1.299013E 00	2.600416E 00	1.789778E 03	7.364029E 02	3
4	7.989893E-01	-2.285220E 03	-1.566308E 03	1.430013E 03	1.299013E 00	2.600416E 00	1.789778E 03	7.364029E 02	4
5	7.989893E-01	-2.285220E 03	-1.566308E 03	1.430013E 03	1.299013E 00	2.600416E 00	1.789778E 03	7.364029E 02	5
6	7.989893E-01	-2.285220E 03	-1.566308E 03	1.430013E 03	1.299013E 00	2.600416E 00	1.789778E 03	7.364029E 02	6
7	7.989893E-01	-2.285220E 03	-1.566308E 03	1.430013E 03	1.299013E 00	2.600416E 00	1.789778E 03	7.364029E 02	7
8	7.989893E-01	-2.285220E 03	-1.566308E 03	1.430013E 03	1.299013E 00	2.600416E 00	1.789778E 03	7.364029E 02	8
9	7.989893E-01	-2.285220E 03	-1.566308E 03	1.430013E 03	1.299013E 00	2.600416E 00	1.789778E 03	7.364029E 02	9
10	7.989893E-01	-2.285220E 03	-1.566308E 03	1.430013E 03	1.299013E 00	2.600416E 00	1.789778E 03	7.364029E 02	10
11	7.989893E-01	-2.285220E 03	-1.566308E 03	1.430013E 03	1.299013E 00	2.600416E 00	1.789778E 03	7.364029E 02	11
12	4.336849E-01	9.636803E 01	9.656773E 01	9.734511E 01	1.400091E 00	1.013705E-01	2.244605E 02	3.565531E 01	12

PT.	H	U	H2O	H2	O2	OH	CO	SUM ALPHAS	
1	4.400000E-04	3.500000E-04	2.000000E-01	2.600000E-02	1.600000E-02	5.600000E-03	5.800000E-01	1.000090E 00	1
2	1.000000E-04	1.000000E-04	2.400000E-01	2.600000E-02	1.000000E-12	1.000000E-12	5.000000E-01	1.000200E 00	2
3	1.000000E-04	1.000000E-04	2.400000E-01	2.600000E-02	1.000000E-12	1.000000E-12	5.000000E-01	1.000200E 00	3
4	1.000000E-04	1.000000E-04	2.400000E-01	2.600000E-02	1.000000E-12	1.000000E-12	5.000000E-01	1.000200E 00	4
5	1.000000E-04	1.000000E-04	2.400000E-01	2.600000E-02	1.000000E-12	1.000000E-12	5.000000E-01	1.000200E 00	5
6	1.000000E-04	1.000000E-04	2.400000E-01	2.600000E-02	1.000000E-12	1.000000E-12	5.000000E-01	1.000200E 00	6
7	1.000000E-04	1.000000E-04	2.400000E-01	2.600000E-02	1.000000E-12	1.000000E-12	5.000000E-01	1.000200E 00	7
8	1.000000E-04	1.000000E-04	2.400000E-01	2.600000E-02	1.000000E-12	1.000000E-12	5.000000E-01	1.000200E 00	8
9	1.000000E-04	1.000000E-04	2.400000E-01	2.600000E-02	1.000000E-12	1.000000E-12	5.000000E-01	1.000200E 00	9
10	1.000000E-04	1.000000E-04	2.400000E-01	2.600000E-02	1.000000E-12	1.000000E-12	5.000000E-01	1.000200E 00	10
11	1.000000E-04	1.000000E-04	2.400000E-01	2.600000E-02	1.000000E-12	1.000000E-12	5.000000E-01	1.000200E 00	11
12	-0.	-0.	-0.	-0.	2.320000E-01	-0.	-0.	1.000000E 00	12

PT	CO2	CHO	HCHO	HYDROCARBON	N2	C-SOLID	STOICH O2	STOICH AIR	
1	1.500000E-01	1.000000E-12	2.000000E-02	-0.	-0.	1.700000E-03	1.879166E 00	8.065155E 00	1
2	1.300000E-01	1.000000E-12	8.700000E-02	-0.	-0.	1.700000E-02	1.968201E 00	8.447284E 00	2
3	1.300000E-01	1.000000E-12	8.700000E-02	-0.	-0.	1.700000E-02	1.968201E 00	8.447284E 00	3
4	1.300000E-01	1.000000E-12	8.700000E-02	-0.	-0.	1.700000E-02	1.968201E 00	8.447284E 00	4
5	1.300000E-01	1.000000E-12	8.700000E-02	-0.	-0.	1.700000E-02	1.968201E 00	8.447284E 00	5
6	1.300000E-01	1.000000E-12	8.700000E-02	-0.	-0.	1.700000E-02	1.968201E 00	8.447284E 00	6
7	1.300000E-01	1.000000E-12	8.700000E-02	-0.	-0.	1.700000E-02	1.968201E 00	8.447284E 00	7
8	1.300000E-01	1.000000E-12	8.700000E-02	-0.	-0.	1.700000E-02	1.968201E 00	8.447284E 00	8
9	1.300000E-01	1.000000E-12	8.700000E-02	-0.	-0.	1.700000E-02	1.968201E 00	8.447284E 00	9
10	1.300000E-01	1.000000E-12	8.700000E-02	-0.	-0.	1.700000E-02	1.968201E 00	8.447284E 00	10
11	1.300000E-01	1.000000E-12	8.700000E-02	-0.	-0.	1.700000E-02	1.968201E 00	8.447284E 00	11

12	-0.		-0.		-0.		-0.	7.680000E-01 -0.	-0.	-0.	12

PT	$\tilde{\alpha}$ ELEM H2	$\tilde{\alpha}$ ELEM O2	$\tilde{\alpha}$ ELEM C	α_{C-F}
1	5.049479E-02	6.502596E-01	2.993390E-01	1.700000E-03
2	5.879727E-02	6.397282E-01	3.016775E-01	1.700000E-02
3	5.879727E-02	6.397282E-01	3.016775E-01	1.700000E-02
4	5.879727E-02	6.397282E-01	3.016775E-01	1.700000E-02
5	5.879727E-02	6.397282E-01	3.016775E-01	1.700000E-02
6	5.879727E-02	6.397282E-01	3.016775E-01	1.700000E-02
7	5.879727E-02	6.397282E-01	3.016775E-01	1.700000E-02
8	5.879727E-02	6.397282E-01	3.016775E-01	1.700000E-02
9	5.879727E-02	6.397282E-01	3.016775E-01	1.700000E-02
10	5.879727E-02	6.397282E-01	3.016775E-01	1.700000E-02
11	5.879727E-02	6.397282E-01	3.016775E-01	1.700000E-02
12	-0.	2.320900E-01	-0.	-0.

UNDRFLOW AT 40106 IN MQ

UNDRFLOW AT 40107 IN AC

UNDRFLOW AT 40115 IN AC

UNDRFLOW AT 40106 IN MQ

UNDRFLOW AT 40107 IN AC AND MQ.

F-1 ENGINE PE/PINF=100 90KF

S= 8.0004824E-01 FT X= 1.8262440E 01 FT Y= 6.5521263E 00 FT PHI= 1.2391614E 00 RAD PHI= 7.1051037E 01 DEG

PSIA= 2.4583333E-01 S/D= 6.9606929E-02 DELSTAR= -9.7495108E 00 DELST-= -2.7568018E 00 DYP/DX= 2.9040000E 00

PRESSURE	LEWIS NUMBER	PRANDTL NUMBER	VISCOSITY	DS	STEP NO
3.5400000E 01	1.0000000E 00	1.0000000E 00	2.6962286E-04	1.2223267E-01	6

R BASE= 0. 6.0000000E 00 1.0000000E 01 1.5000000E 01

Q BASE= -7.8072448 4E-04 -7.1146334 4E-04 -4.7610443 8E-04 -3.4759458 3E-04

PT.	PSI	VELOCITY	TEMPERATURE	VISCOSITY	DENSITY	N	MOLEC. WT.	RHO-U	
1	9.161500E 01	1.400000E 04	6.000000E 02	2.696229E-04	1.316434E-05	-4.361152E 00	1.991723E 01	1.843007E-01	1
2	9.176000E 01	1.399999E 04	6.000020E 02	2.696229E-04	1.316429E-05	-4.241075E 00	1.991723E 01	1.843000E-01	2
3	9.190500E 01	1.399774E 04	6.004805E 02	2.696229E-04	1.315381E-05	-4.120941E 00	1.991710E 01	1.841236E-01	3
4	9.205000E 01	1.382710E 04	6.361878E 02	2.696229E-04	1.241574E-05	-3.996390E 00	1.990667E 01	1.716738E-01	4
5	9.219500E 01	6.219915E 03	8.928414E 02	2.696229E-04	8.853657E-06	-3.731004E 00	1.945274E 01	5.506899E-02	5
6	9.234000E 01	6.001150E 03	8.897706E 02	2.696229E-04	8.884412E-06	-3.322537E 00	1.943999E 01	5.331669E-02	6
7	9.248500E 01	6.000003E 03	8.897533E 02	2.696229E-04	8.884586E-06	-2.907430E 00	1.943992E 01	5.330754E-02	7
8	9.263000E 01	6.000000E 03	8.897525E 02	2.696229E-04	8.884594E-06	-2.492288E 00	1.943992E 01	5.330756E-02	8
9	9.277500E 01	6.000000E 03	8.897517E 02	2.696229E-04	8.884602E-06	-2.077146E 00	1.943992E 01	5.330761E-02	9
10	9.292000E 01	6.000000E 03	8.897510E 02	2.696229E-04	8.884609E-06	-1.662004E 00	1.943992E 01	5.330765E-02	10
11	9.306500E 01	6.000000E 03	8.897503E 02	2.696229E-04	8.884616E-06	-1.246863E 00	1.943992E 01	5.330769E-02	11
12	9.321000E 01	5.999999E 03	8.897496E 02	2.696229E-04	8.884623E-06	-8.317221E-01	1.943992E 01	5.330773E-02	12
13	9.335500E 01	5.999792E 03	8.897585E 02	2.696229E-04	8.884630E-06	-4.165741E-01	1.944015E 01	5.330593E-02	13
14	9.350000E 01	5.958836E 03	8.916274E 02	2.696229E-04	8.884948E-06	0.	1.948426E 01	5.294395E-02	14
15	9.364500E 01	1.330406E 02	2.315240E 02	2.696229E-04	4.915387E-05	1.901049E 00	2.877130E 01	6.539461E-03	15
16	9.379000E 01	1.000129E 02	2.240029E 02	2.696229E-04	5.093031E-05	5.765419E 00	2.884926E 01	5.093688E-03	16
17	9.393500E 01	1.000000E 02	2.240000E 02	2.696229E-04	5.093101E-05	1.011030E 01	2.884928E 01	5.093101E-03	17

PT.	SPECIFIC HEAT	STATIC H	TOTAL H	SENSE TOT H	GAMMA	MACH NUMBER	TOTAL T	TOTAL P	PT
1	7.057805E-01	-2.314211E 03	1.599869E 03	4.337549E 03	1.341092E 00	7.361793E 00	6.145748E 03	3.324647E 05	1
2	7.057808E-01	-2.314210E 03	1.599864E 03	4.337545E 03	1.341092E 00	7.361776E 00	6.145739E 03	3.324599E 05	2
3	7.058079E-01	-2.313944E 03	1.598874E 03	4.336678E 03	1.341039E 00	7.357782E 00	6.143753E 03	3.313515E 05	3
4	7.125397E-01	-2.294134E 03	1.523868E 03	4.271311E 03	1.337006E 00	7.069966E 00	5.994489E 03	2.593131E 05	4
5	7.984397E-01	-2.278848E 03	-1.506270E 03	1.485458E 03	1.299024E 00	2.692310E 00	1.860452E 03	8.592710E 02	5
6	7.989367E-01	-2.285354E 03	-1.566166E 03	1.430059E 03	1.299037E 00	2.601230E 00	1.789953E 03	7.374015E 02	6
7	7.989390E-01	-2.285389E 03	-1.566476E 03	1.429772E 03	1.299037E 00	2.600754E 00	1.789588E 03	7.368114E 02	7
8	7.989369E-01	-2.285390E 03	-1.566477E 03	1.429771E 03	1.299037E 00	2.600753E 00	1.789587E 03	7.368112E 02	8
9	7.989387E-01	-2.285390E 03	-1.566478E 03	1.429770E 03	1.299037E 00	2.600754E 00	1.789586E 03	7.368124E 02	9
10	7.989386E-01	-2.285391E 03	-1.566478E 03	1.429769E 03	1.299037E 00	2.600755E 00	1.789586E 03	7.368136E 02	10
11	7.989384E-01	-2.285391E 03	-1.566479E 03	1.429768E 03	1.299037E 00	2.600756E 00	1.789585E 03	7.368147E 02	11
12	7.989383E-01	-2.285392E 03	-1.566479E 03	1.429768E 03	1.299037E 00	2.600757E 00	1.789585E 03	7.368156E 02	12
13	7.989290E-01	-2.285291E 03	-1.566428E 03	1.429717E 03	1.299037E 00	2.600669E 00	1.789542E 03	7.367065E 02	13
14	7.971286E-01	-2.265355E 03	-1.556273E 03	1.419824E 03	1.299033E 00	2.583138E 00	1.781173E 03	7.153302E 02	14
15	4.350250E-01	8.384729E 01	8.420075E 01	1.010722E 02	1.399879E 00	1.324850E-01	2.323366E 02	3.586682E 01	15
16	4.336853E-01	9.636311E 01	9.656286E 01	9.734653E 01	1.400091E 00	1.013828E-01	2.244635E 02	3.565537E 01	16
17	4.336849E-01	9.636803E 01	9.656773E 01	9.734511E 01	1.400091E 00	1.013705E-01	2.244605E 02	3.565531E 01	17

PT.	H	O	H2O	H2	O2	OH	CO	SUM ALPHAS	
1	4.400000E-04	3.500000E-04	2.000000E-01	2.600000E-02	1.600000E-02	5.600000E-03	5.800000E-01	1.000090E 00	1
2	4.399995E-04	3.499997E-04	2.000000E-01	2.600000E-02	1.599998E-02	5.599992E-03	5.799999E-01	1.000090E 00	2
3	4.399040E-04	3.499294E-04	2.000113E-01	2.600000E-02	1.599548E-02	5.598418E-03	5.799774E-01	1.000090E 00	3
4	4.326519E-04	3.445970E-04	2.008644E-01	2.600000E-02	1.565421E-02	5.478973E-03	5.782710E-01	1.000092E 00	4
5	1.093464E-04	1.068723E-04	2.389004E-01	2.599999E-02	4.398297E-04	1.539404E-04	5.021990E-01	1.000197E 00	5
6	1.000489E-04	1.000359E-04	2.399942E-01	2.600000E-02	2.299909E-06	8.049687E-07	5.000114E-01	1.000200E 00	6
7	1.000001E-04	1.000001E-04	2.399999E-01	2.600000E-02	5.855711E-09	2.050149E-09	5.000000E-01	1.000200E 00	7
8	9.999998E-05	9.999998E-05	2.400000E-01	2.600000E-02	8.393809E-12	3.587833E-12	4.999999E-01	1.000200E 00	8
9	9.999998E-05	9.999998E-05	2.400000E-01	2.600000E-02	1.003709E-12	1.001298E-12	4.999999E-01	1.000200E 00	9
10	9.999998E-05	9.999998E-05	2.400000E-01	2.600000E-02	1.013160E-12	9.999998E-13	4.999999E-01	1.000200E 00	10
11	9.999998E-05	9.999998E-05	2.400000E-01	2.599999E-02	2.720565E-11	9.999998E-13	4.999999E-01	1.000200E 00	11
12	9.999997E-05	9.999997E-05	2.399999E-01	2.599999E-02	2.076384E-08	9.999997E-13	4.999999E-01	1.000200E 00	12
13	9.999645E-05	9.999645E-05	2.399915E-01	2.599908E-02	8.190783E-06	9.999645E-13	4.999823E-01	1.000200E 00	13
14	9.930230E-05	9.930230E-05	2.383255E-01	2.581860E-02	1.618624E-03	9.930230E-13	4.965115E-01	1.000198E 00	14

15	5.600103E-07	5.600103E-07	1.344025E-03	1.456027E-04	2.307007E-01	5.600103E-15	2.800052E-03	1.000001E 00	15
16	2.188652E-10	2.188652E-10	5.252765E-07	5.690495E-08	2.319995E-01	2.188652E-18	1.094326E-06	9.999999E-01	16
17	-0.	-0.	-0.	-0.	2.320000E-01	-0.	-0.	1.000000E 00	17

PT	CO2	CHO	HCHO	HYDROCARBON	N2	C-SOLID	STOICH O2	STOICH AIR	
1	1.500000E-01	1.000000E-12	2.000000E-02	-0.	-0.	1.700000E-03	1.879166E 00	8.065155E 00	1
2	1.500000E-01	1.000000E-12	2.000009E-02	-0.	-0.	1.700020E-03	1.879166E 00	8.065156E 00	2
3	1.499943E-01	9.999999E-13	2.001891E-02	-0.	-0.	1.704320E-03	1.879191E 00	8.065261E 00	3
4	1.495677E-01	9.999998E-13	2.144800E-02	-0.	-0.	2.030662E-03	1.881060E 00	8.073282E 00	4
5	1.305498E-01	9.999998E-13	8.515820E-02	-0.	-0.	1.657941E-02	1.965715E 00	8.436611E 00	5
6	1.300029E-01	9.999998E-13	8.699036E-02	-0.	-0.	1.699780E-02	1.968188E 00	8.447268E 00	6
7	1.300000E-01	9.999998E-13	8.699996E-02	-0.	-0.	1.699999E-02	1.968201E 00	8.447284E 00	7
8	1.300000E-01	9.999998E-13	8.699999E-02	-0.	-0.	1.700000E-02	1.968201E 00	8.447284E 00	8
9	1.300000E-01	9.999998E-13	8.699999E-02	-0.	-0.	1.700000E-02	1.968201E 00	8.447284E 00	9
10	1.300000E-01	9.999998E-13	8.699999E-02	-0.	4.356625E-14	1.700000E-02	1.968201E 00	8.447284E 00	10
11	1.300000E-01	9.999998E-13	8.699999E-02	-0.	8.674975E-11	1.700000E-02	1.968201E 00	8.447284E 00	11
12	1.300000E-01	9.999997E-13	8.699998E-02	-0.	6.873216E-08	1.700000E-02	1.968201E 00	8.447282E 00	12
13	1.299954E-01	9.999645E-13	8.699692E-02	-0.	2.711431E-05	1.699940E-02	1.968176E 00	8.446818E 00	13
14	1.290930E-01	9.930230E-13	8.639300E-02	-0.	5.358203E-03	1.688139E-02	1.963199E 00	8.355519E 00	14
15	7.280134E-04	5.600103E-15	4.872090E-04	-0.	7.636990E-01	9.520175E-05	3.009676E-02	3.032395E-02	15
16	2.845248E-07	2.188652E-18	1.904127E-07	-0.	7.679982E-01	3.720708E-08	1.187824E-05	1.182741E-05	16
17	-0.	-0.	-0.	-0.	7.680000E-01	-0.	-0.	-0.	17

PT	ELEM H2	ELEM O2	ELEM C	
1	5.049479E-02	6.502596E-01	2.993390E-01	1.700000E-03
2	5.049480E-02	6.502596E-01	2.993390E-01	1.700020E-03
3	5.049713E-02	6.502600E-01	2.993396E-01	1.704320E-03
4	5.067421E-02	6.500319E-01	2.993895E-01	2.030662E-03
5	5.856903E-02	6.400176E-01	3.016131E-01	1.657941E-02
6	5.879607E-02	6.397296E-01	3.016771E-01	1.699780E-02
7	5.879726E-02	6.397281E-01	3.016774E-01	1.699999E-02
8	5.879726E-02	6.397281E-01	3.016774E-01	1.700000E-02
9	5.879726E-02	6.397281E-01	3.016774E-01	1.700000E-02
10	5.879726E-02	6.397281E-01	3.016774E-01	1.700000E-02
11	5.879726E-02	6.397281E-01	3.016774E-01	1.700000E-02
12	5.879725E-02	6.397281E-01	3.016774E-01	1.700000E-02
13	5.879518E-02	6.397137E-01	3.016668E-01	1.699940E-02
14	5.838704E-02	6.368834E-01	2.995727E-01	1.688139E-02
15	3.292708E-04	2.342833E-01	1.689425E-03	9.520175E-05
16	1.286868E-07	2.320009E-01	6.602670E-07	3.720708E-08
17	-0.	2.320000E-01	-0.	-0.

APPENDIX B

PLUME SAMPLE CALCULATIONS

As was described in section Vc, by using the data in Reference 27, with a little help from the equilibrium calculations of Reference 33, it was possible to determine what is hoped to be a reasonable approximation of the chemical composition of the plume core and turbine exhaust gas-boundary layer region, at the nozzle exit. The mass fractions are given below in Table B-I.

It was decided to run two basic test cases. Case A was at sea level pressure, with the plume exhausting into essentially quiescent air (u_∞ = 100 ft./sec.).

Since photographs in Reference 27 of sea level tests of various rocket engine exhausts did not show any pronounced pluming for several diameters downstream of the exit, it was decided to arbitrarily incline the plume boundary streamline at 1^o to the axis. Since no definite temperature or velocity distributions were available it was necessary to make what seemed to be reasonable approximations. The values of T, M, and u are given below in Table B-II.

Case A was run with both finite-rate chemistry (including the solid carbon global oxidation model) and frozen chemistry, and the results presented in Figures 6, 21, and 22. The fact that the

radiation base heat transfer levels of the chemically frozen calculation were near those of the reacting calculation shows that the solid carbon was being burnt quickly enough to almost compensate for the radiation increase due to higher temperatures in the chemically reacting flow field.

Case B was designed to have $P_{exit}/P_{\infty} = 100$. Reference 34 could be used to describe the plume boundary streamline coordinates, provided that the air was again considered to be quiescent. The initial plume angle (φ) was 71^{o}, and the temperature and velocity of case A were adjusted to turn through this angle. The resulting temperatures were low enough so that the plume would be chemically frozen until far downstream of the exit. Thus, it was not necessary to make a finite rate chemistry run for case B. The base heat transfer flux is shown in Figure 7 for this case.

TABLE B-I

PLUME CHEMICAL COMPOSITION (MASS FRACTIONS)

Specie	Flow Region: Core	T.E.G. - B.L.	Air
H	4.4×10^{-4}	1×10^{-4}	0
O	3.5×10^{-4}	1×10^{-4}	0
H_2O	.20	.24	0
H_2	.026	.026	0
O_2	.016	1×10^{-12}	.232
OH	.0056	1×10^{-12}	0
CO	.58	.50	0
CO_2	.15	.13	0
CHO	1×10^{-12}	1×10^{-12}	0
HCHO	.02	.087	0
C_9H_{20}	0	0	0
N_2	0	0	.768
$C_{(solid)}$	.0017	.017	0

TABLE B-II

CALCULATION INITIAL CONDITIONS

		Core	T.E.G. - B.L.	Air
Case A	$T(^{o}K)$	1900	1500	289
P=2116 psfa	M	3.55	.96	.09
$\varphi = 1^{o}$	$u\left(\frac{ft}{sec}\right)$	11,640	2820	100
Case B	$T(^{o}K)$	600	890	224
P=35.4 psfa	M	7.36	2.60	.10
$\varphi = 71^{o}$	$u\left(\frac{ft}{sec}\right)$	14,000	6000	100

APPENDIX C

CHEMICAL SPECIES AND ELEMENTARY KINETIC REACTIONS

There are 12 gaseous and 1 solid specie in the chemical system: H, O, H_2O, H_2, O_2, OH, CO, CO_2, CHO, HCHO, C_nH_{2n+2}, N_2, and $C_{(solid)}$. The global reactions involving C_nH_{2n+2} and $C_{(solid)}$ have already been described in detail. The global reactions are used in conjunction with the elementary chemical kinetic reactions of Reference 3, which are tabulated below in Table C-I. The chemical reactions were linearized in the manner described in References 35 and 36, and the resulting system of equations is solved using the technique of Reference 37.

TABLE C-I

Reaction	Forward Reaction Rate	Backward Reaction Rate
$HCHO+OH \rightleftarrows CHO+H_2O$	3.0×10^{13}	$1.0\times10^{12}(T)^{.31}\ e^{-39,510/RT}$
$HCHO+H \rightleftarrows CHO+H_2$	$1.7\times10^{13}\ e^{-3000/RT}$	$8.5\times10^{10}(T)^{.37}\ e^{-27,720/RT}$
$HCHO+O \rightleftarrows CHO+OH$	3.0×10^{13}	$1.0\times10^{11}(T)^{.31}\ e^{-76,570/RT}$
$CHO+O \rightleftarrows CO+OH$	$5.4\times10^{11}(T)^{.5}$	$7.0\times10^{10}(T)^{.5}\ e^{-73,800/RT}$
$CHO+OH \rightleftarrows CO+H_2O$	3.0×10^{13}	$7.0\times10^{13}(T)^{.29}\ e^{-93,600/RT}$
$CO+OH \rightleftarrows CO_2+H$	$3.2\times10^{12}\ e^{-6300/RT}$	$2.7\times10^{17}(T)^{-.79}\ e^{-30,700/RT}$
$OH+H_2 \rightleftarrows H+H_2O$	$6.3\times10^{13}\ e^{-5900/RT}$	$2.4\times10^{14}\ e^{-20,690/RT}$
$2OH \rightleftarrows H_2O+O$	$7.6\times10^{12}\ e^{-1000/RT}$	$6.9\times10^{13}\ e^{-17,740/RT}$
$O+H_2 \rightleftarrows OH+H$	$3.3\times10^{12}\ e^{-7140/RT}$	$1.4\times10^{12}\ e^{-5190/RT}$
$H+O_2 \rightleftarrows OH+O$	$2.4\times10^{14}e^{-16,750/RT}$	$3.2\times10^{11}(T)^{.47}\ e^{-100/RT}$
$O+H+M \rightleftarrows OH+M$	3.0×10^{14}	$7.5\times10^{14}(T)^{.06}\ e^{-101,290/RT}$
$2O+M \rightleftarrows O_2+M$	2.2×10^{13}	$2.5\times10^{16}(T)^{-.5}\ e^{-117,900/RT}$
$2H+M \rightleftarrows H_2+M$	$2.0\times10^{18}(T)^{-1.0}$	$2.4\times10^{19}(T)^{-.86}\ e^{-103,240/RT}$
$H+OH+M \rightleftarrows H_2O+M$	$2.3\times10^{21}(T)^{-1.5}$	$1.2\times10^{23}(T)^{-1.34}\ e^{-118,027/RT}$

BIBLIOGRAPHY

1. Edelman, R. and Fortune, O., "Mixing and Combustion in the Exhaust Plumes of Rocket Engines Burning RP1 and Liquid Oxygen," GASL TR 631, November 1966.

2. Slutsky, S. and Melnick, J.D., "Radiation From Carbon in a Rocket Plume Mixing Region with Coupled Convective and Radiative Energy Fluxes and General Optical Thickness," GASL TR 628, September 1966.

3. Chinitz, W. and Baurer, T., "An Analysis of Non-Equilibrium Hydrocarbon-Air Combustion, Part I - Chemical Kinetics," GASL TR 546, August 1965.

4. Schlichting, H., "Boundary Layer Theory," Fourth Edition, McGraw-Hill, New York, 1960.

5. Ferriso, C.C., Ludwig, C.B., and Huffaker, R.M., "Continuous Carbon Absorption Studies," N66-22334, FF No. 672, August 1965.

6. Vidale, G.L., "The Vaporization of Graphite, TiC, ZrC, and H_fC," General Electric Space Sciences Laboratory R61SD010, January 1961.

7. Nolan, E.J. and Scala, S.M., "Aerothermodynamic Behavior of Pyrolytic Graphite During Sustained Hypersonic Flight," ARS Journal, pp. 26-35, January 1962.

8. Scala, S.M., "The Ablation of Graphite in Dissociated Air, Part I - Theory," IAS paper 62-154, June 1962.

9. Scala, S.M. and Gilbert, L.M., "Aerothermochemical Behavior of Graphite at Elevated Temperatures," General Electric Space Sciences Laboratory R63SD89, November 1963.

10. Scala, S.M. and Gilbert, L,M., " The Sublimation of Graphite at Hypersonic Speeds," General Electric Space Sciences Laboratory R64SD55, August 1964.

11. Essenhigh, R.H., Froberg, R., and Howard, J.B., "Predicted Burning Rates of Single Carbon Particles," Presented before American Chemical Society Division of Fuel Chemistry, MS 64-479, April 1964.

12. Gregg, S.J. and Tyson, R.F.S., "The Kinetics of Oxidation of Carbon and Graphite by Oxygen at 500°-600° C," Carbon, Vol. 3, pp. 39-42, 1965.

13. Golvina, E.S. and Khaustovich, G.P.K., "The Interaction of Carbon with Carbon Dioxide and Oxygen at Temperatures up to 3000°K," Eight Symposium (International) on Combustion, pp. 784-792, August 1960.

14. Krieger, F.J., "The Thermodynamics of the Graphite-Carbon Vapor System," Rand RM-3326-1-PR, December 1965.

15. Ong, J.N., "On the Kinetics of Oxidation of Graphite," Carbon, Vol. 2, pp. 281-297, 1964.

16. Walls, J.R. and Strickland-Constable, R.F., "Oxidation of Carbon Between 1000-2400°C," Carbon, Vol. 1, pp. 333-338, 1964.

17. Galbransen, E.A., Andrew, K.F. and Brassart, F.A., "Ablation of Graphite in Oxygen and Air at 1000-1400°C under Flow Conditions," Carbon, Vol. 1, pp. 413-424, 1964.

18. Galbransen, E.A., Andrew, K.F., and Brassart, F.A., "Reaction of Graphite with Carbon Dioxide at 1000-1600°C under Flow Conditions," Carbon, Vol. 2, pp. 421-429, 1965.

19. Tesner, P.A., "Formation of Dispersed Carbon by Thermal Decomposition of Hydrocarbons," Seventh Symposium (International) on Combustion, pp. 546-553, 1959.

20. Tesner, P.A., "The Activation Energy of Gas Reactions with Solid Carbon," Eighth Symposium (International) on Combustion, pp. 807-814, August, 1960.

21. Homann, K.H., "Carbon Formation in Premixed Flames," Combustion and Flame, Vol. 11, pp. 267-287, August 1967.

22. "Reaction Times of Hydrocarbon Oxidation Behind Incident Shock Waves in a Shock Tube," Technical Performance Status Reports, February 15 to September 15, 1967, General Dynamics/Convair, Air Force Aero Propulsion Laboratory Contract No. F33615-67-C-1382, Wright Patterson Air Force Base.

23. Nixon, A.C., et. al., "Vaporizing and Endothermic Fuels for Advanced Engine Application," Shell Development Company, APL-TDR 64-100, Parts II and III, and AFAPL-TR-67-114, Part I, 1964 through 1967.

24. Burwell, W.G. and Olson, D.R., "The Spontaneous Ignition of Isooctane Air Mixtures under Steady Flow Conditions," Presented at the SAE Meeting, May 1965, Paper 650510.

25. Salooja, K.C., Combustion and Flame, V. 4, p. 117, 1960.

26. Rifkin, E.B. and Walcutt, C., SAE Transactions Vol. 65, p. 552, 1957.

27. Cline, G.L., et. al., "Radiation and Structural Characteristics of Rocket Engine Exhaust Plumes," Rocketdyne R-6742, September 1966.

28. Thomson, J. D., "A Study of Radiative Properties and Composition of the Turbine Exhaust Products in the F-1 Engine," Rocketdyne R6743, September 1966.

29. Hawthorn, R.D. and Nixon, A.C., "Shock Tube Ignition Delay Studies of Endothermic Fuels," AIAA Journal Vol. 4, pp. 513-520, March 1966.

30. Fristrom, R.M. and Westenberg, A.A., "Flame Structure," McGraw-Hill, New York, 1965.

31. Echigo, R., Nishiwaki, N., and Hirata, M., "A Study on the Radiation of Luminous Flames," Eleventh Symposium (International) on Combustion, August 1966.

32. Lee, K.B., Thring, M.W., and Beér, J.M., "On The Rate of Combustion of Soot in a Laminar Soot Flame," Combustion and Flame, V. 6, pp. 137-145, 1962.

33. Private Communication from Dr. R. Farmer to Dr. S. Slutsky, April 6, 1966.

34. Andrews, E.H., Vick, A.R., and Craidon, C.B., "Theoretical Boundaries and Internal Characteristics of Exhaust Plumes from Three Different Supersonic Nozzles," NASA TN D-2650, March 1965,

35. Moretti, G., "A New Technique for the Numerical Analysis of Nonequilibrium Flows," AIAA Journal, V. 3, pp. 223-229, February 1965.

36. Hoffman, J.R. and Wecker, M.S., "Program Generation for Finite-Rate Chemical Systems," GASL TR 575, March 1966.

37. Magnus, D.E. and Schechter, H.S., "Analysis of Error Growth and Stability for the Numerical Integration of the Equations of Chemical Kinetics," GASL TR 607, June 1966.

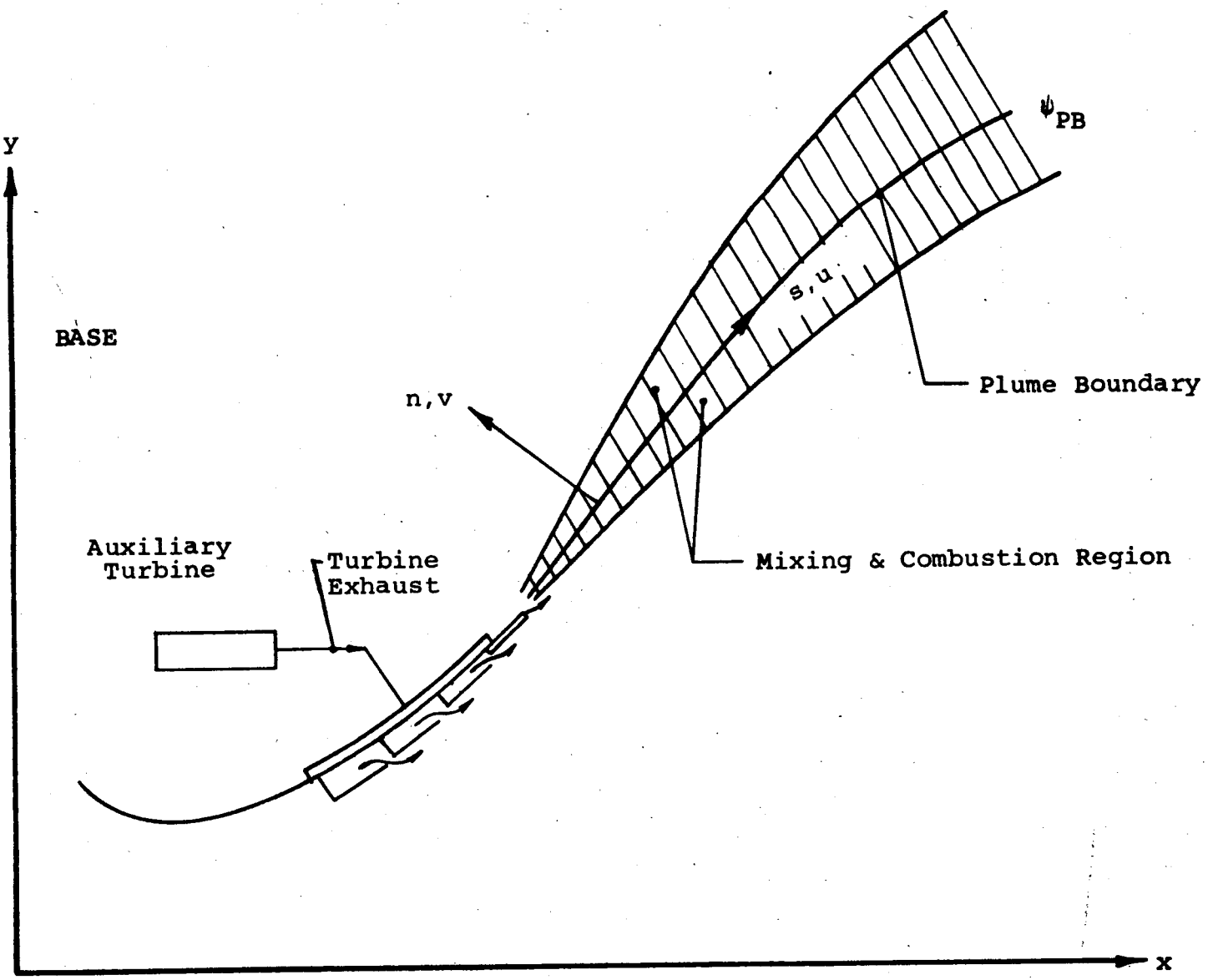

FIGURE 1 - SCHEMATIC OF FLOW FIELD

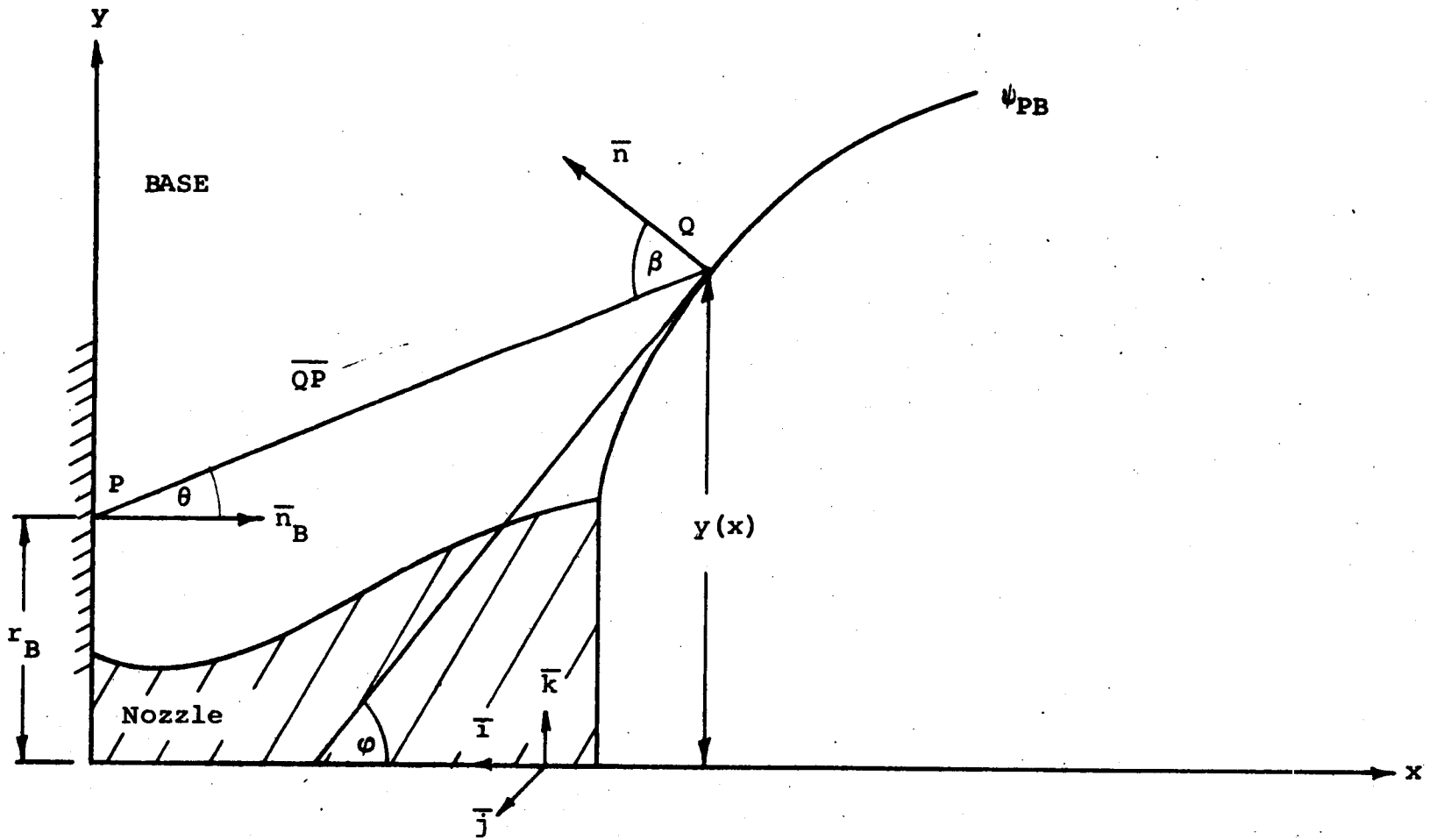

FIGURE 2 - SCHEMATIC OF F-1 ENGINE AND PLUME

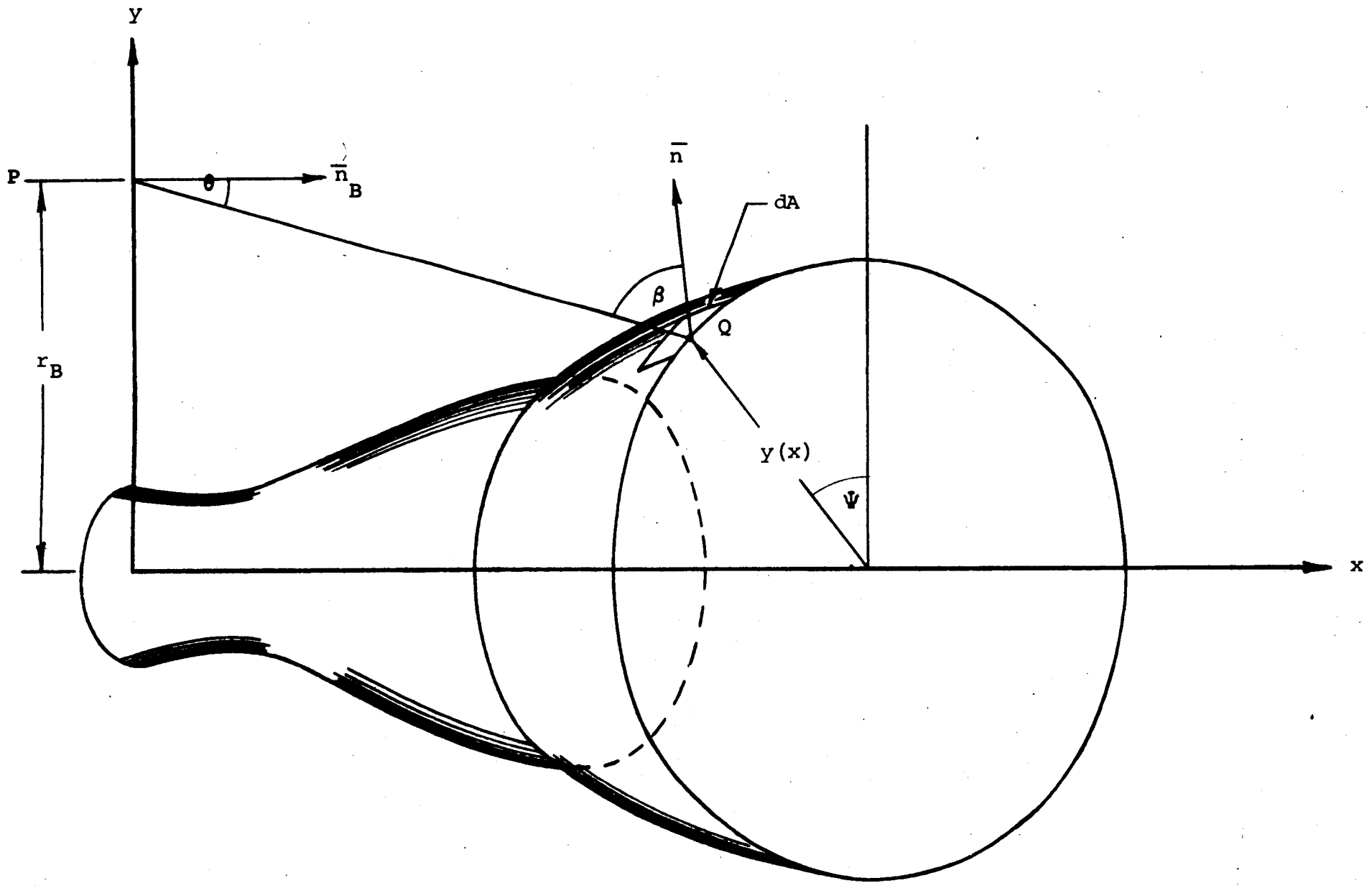

FIGURE 3 - SKETCH OF F-1 ENGINE AND PLUME

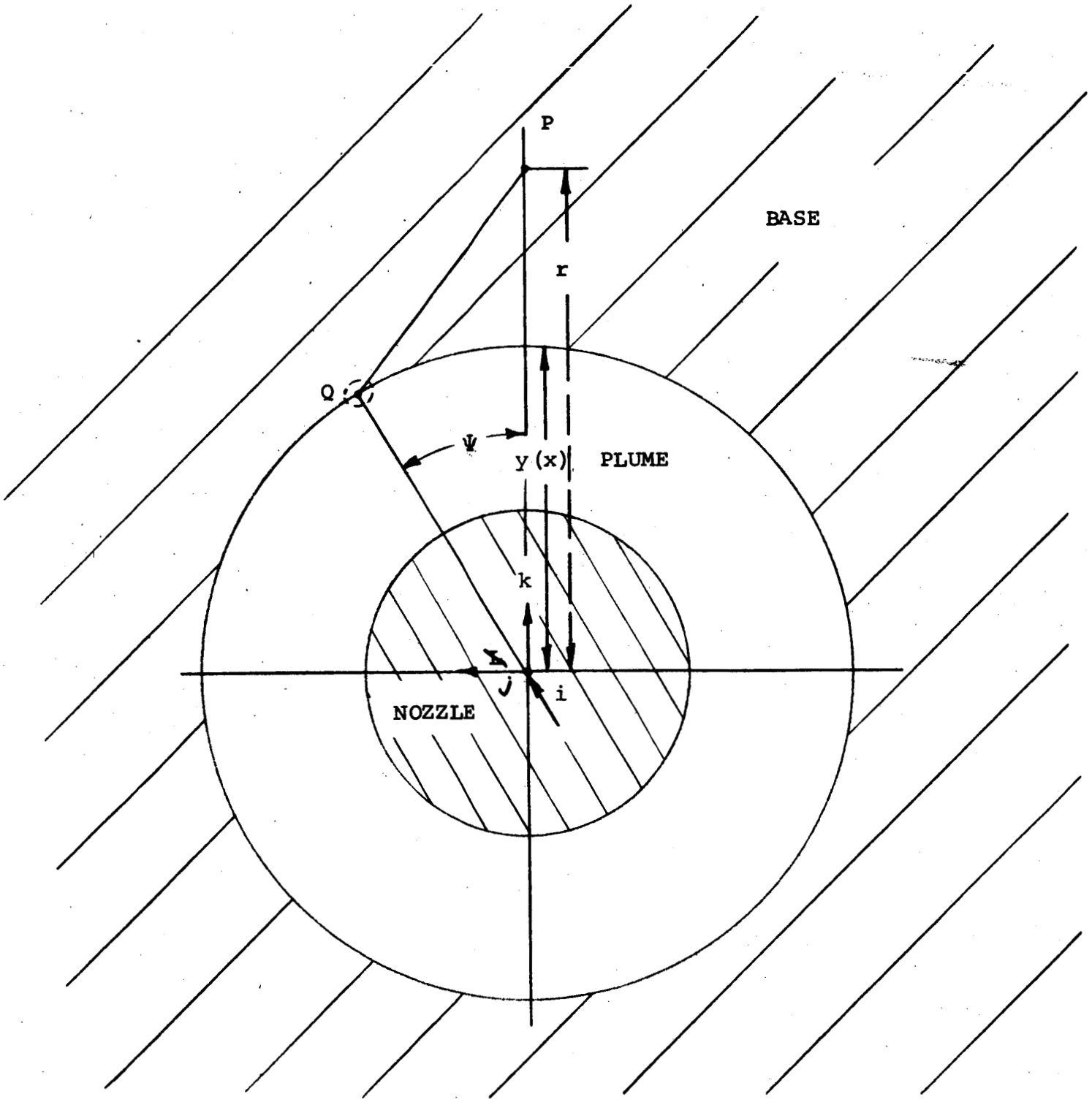

FIGURE 4 - FRONT VIEW OF PLUME AND BASE

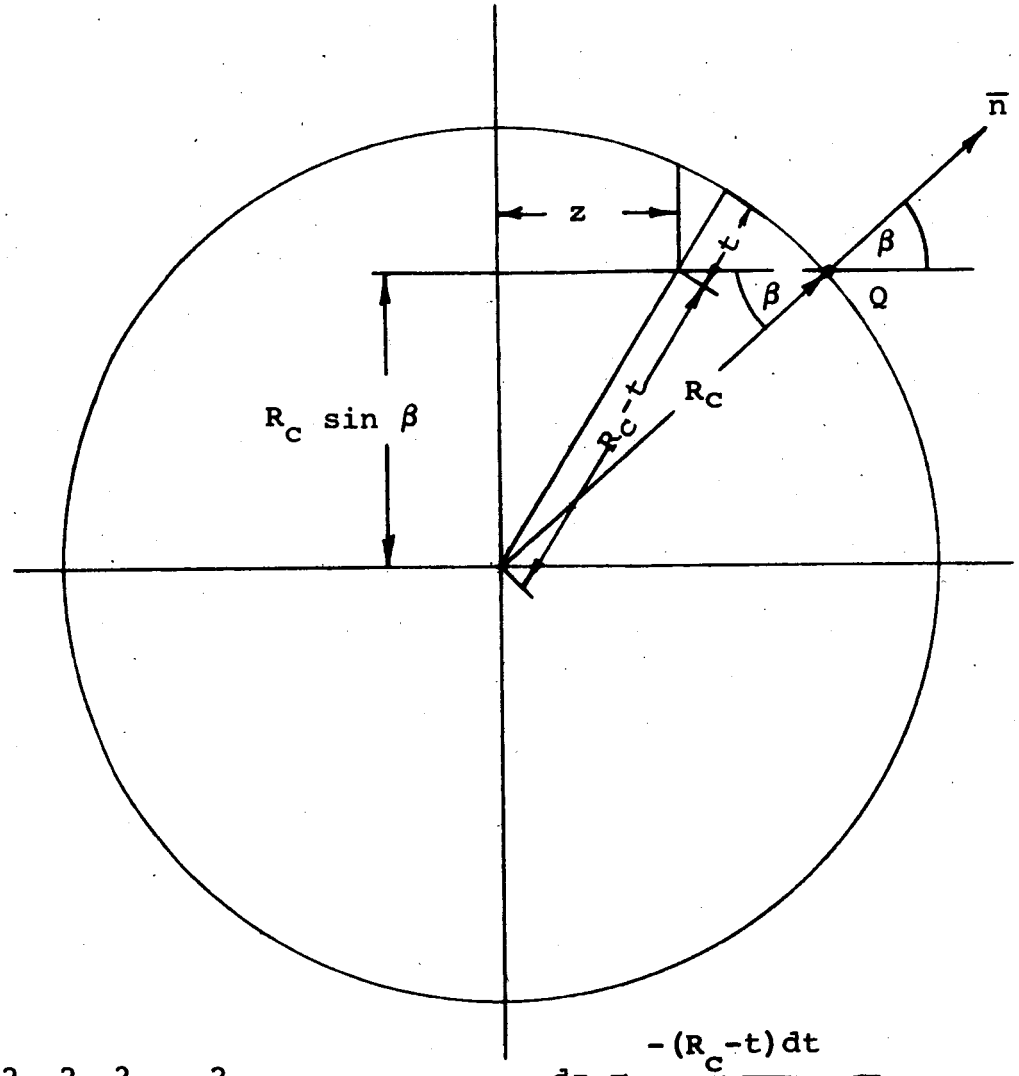

$$(R_c-t)^2=z^2+R_c^2 \sin^2\beta$$

$$-2(R_c-t)dt = 2zdz$$

$$dz = \frac{-(R_c-t)dt}{z}$$

$$dz = \frac{-(R_c-t)dt}{\sqrt{(R_c-t)-R_c^2 \sin^2\beta}}$$

$$dz = \frac{-(R_c-t)dt}{\sqrt{(R_c\cos\beta)^2-(2R_c+t)t}}$$

FIGURE 5 - RAY PASSAGE THROUGH PLUME SECTION

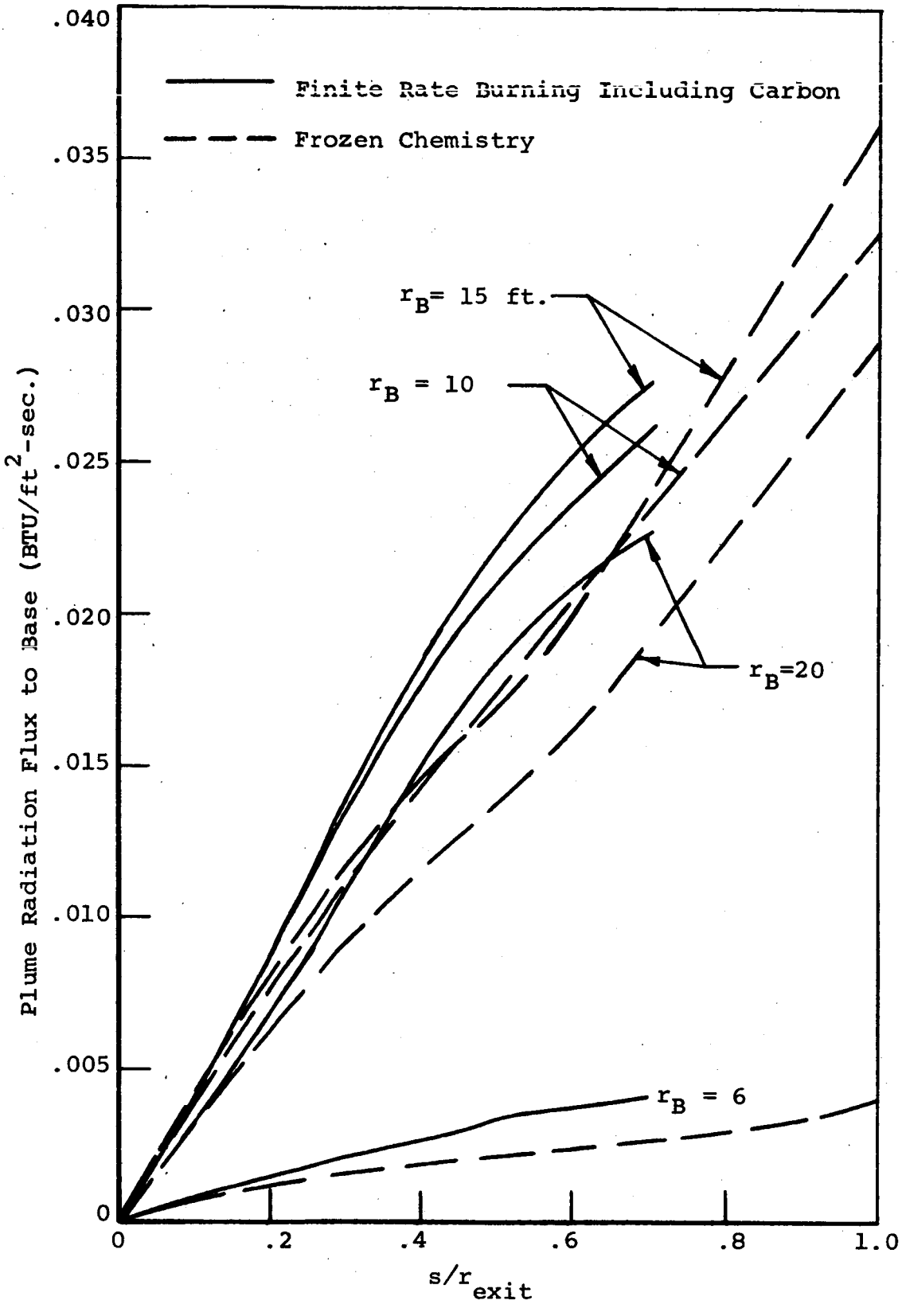

FIGURE 6 - CUMULATIVE BASE RADIATION HEAT FLUX

CASE A SEA LEVEL

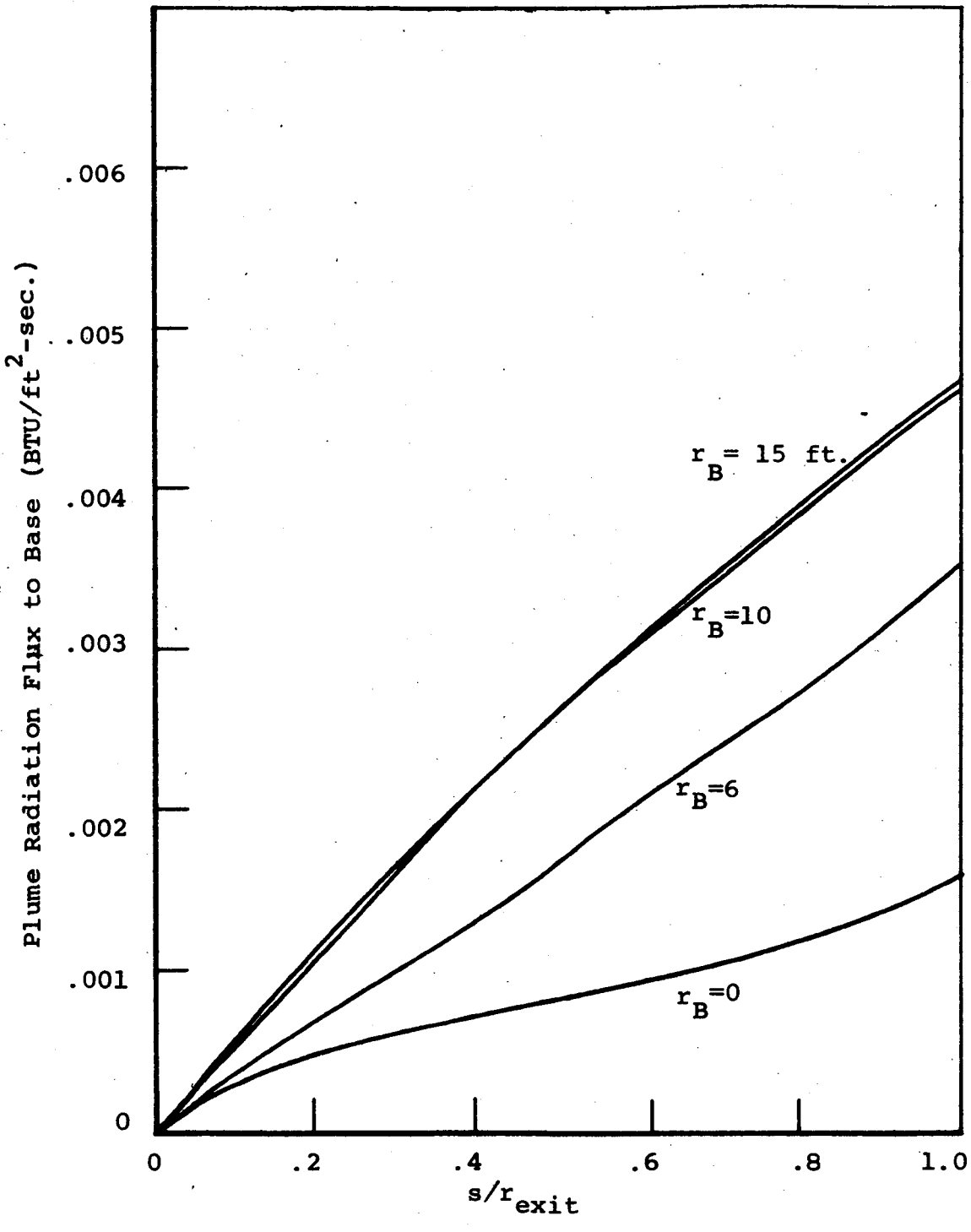

FIGURE 7 - CUMULATIVE BASE RADIATION HEAT FLUX
CASE B FROZEN CHEMISTRY

REACTION SUBSYSTEMS FOR THE OXIDATION OF PROPANE

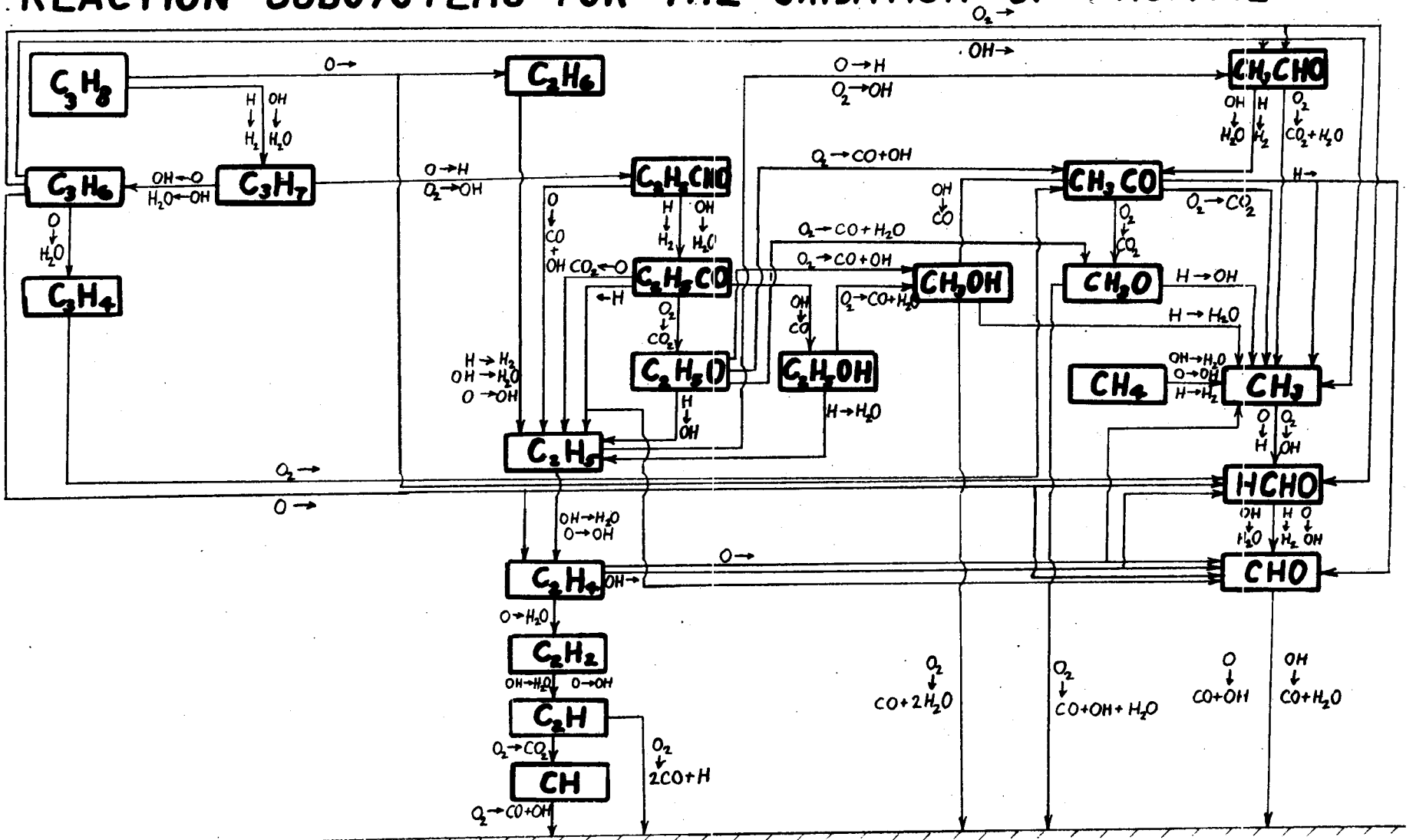

EQUILIBRIUM PRODUCTS: H_2, H, O_2, O, H_2O, OH, CO, CO_2

FIGURE 8

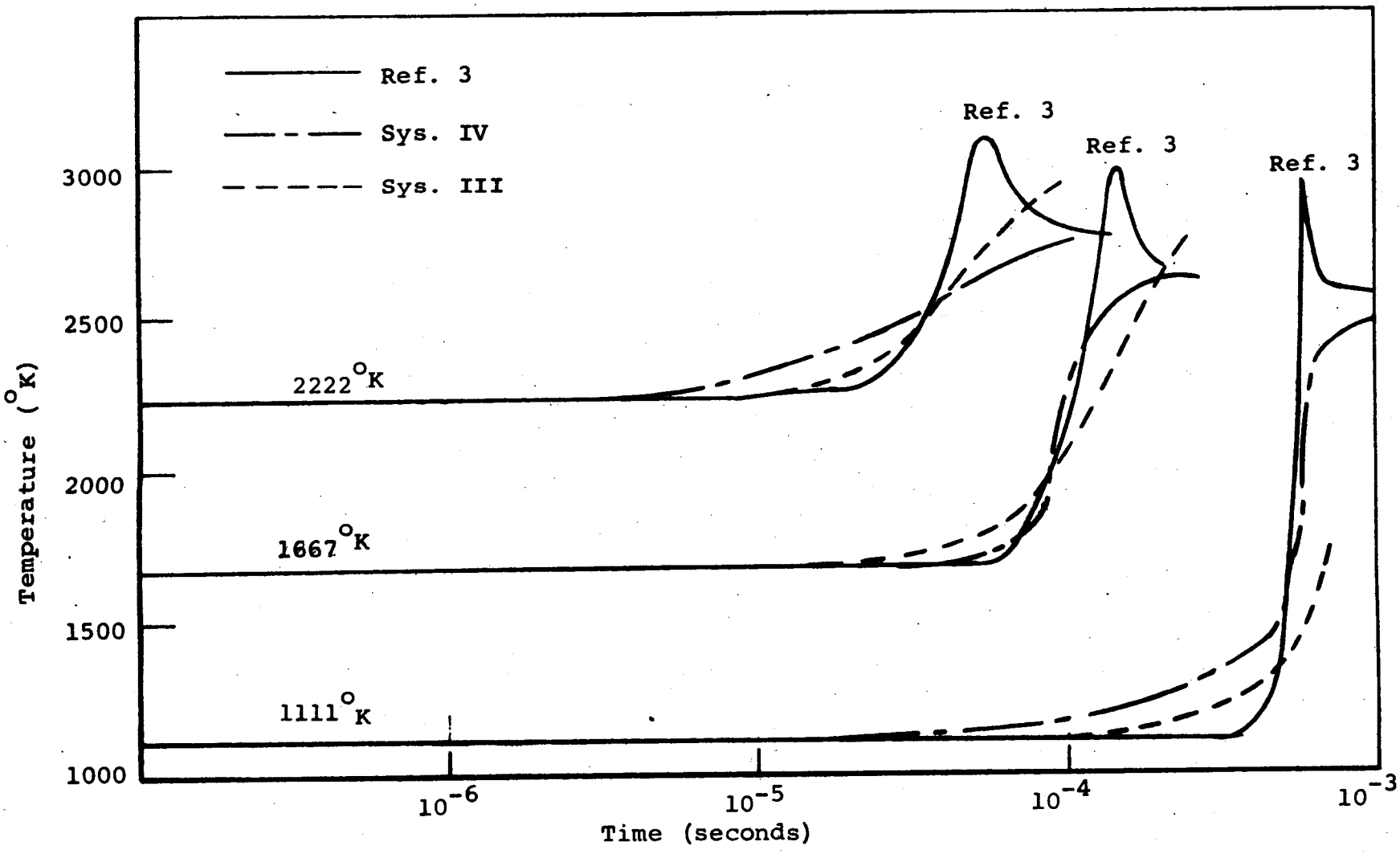

FIGURE 9 - COMPARISON OF SYSTEM IV WITH RESULTS OF REF. 3 AND SYSTEM III FOR DIFFERENT TEMPERATURES

P = 1 Atm. $\varphi = 1$

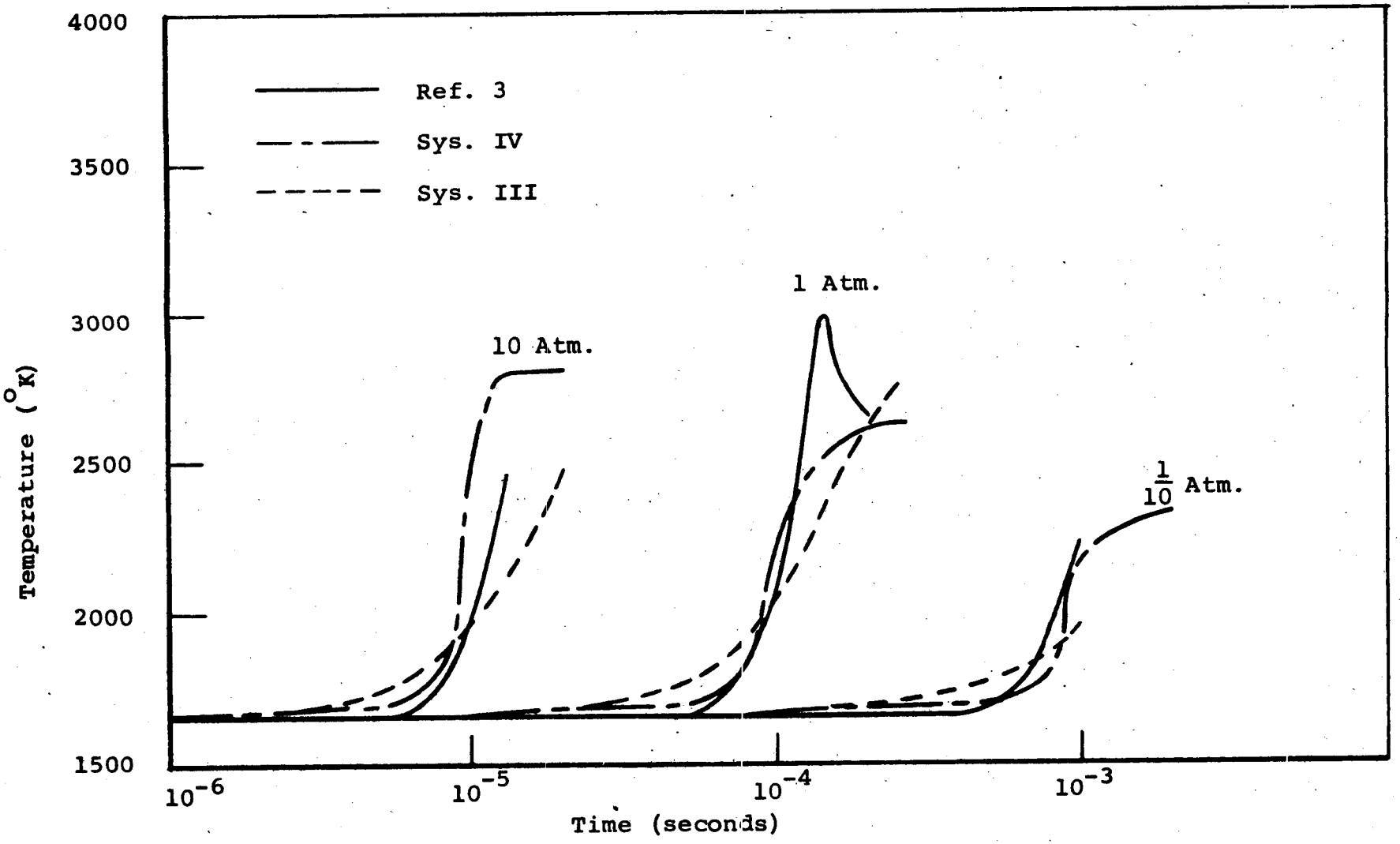

FIGURE 10 - COMPARISON OF SYSTEM IV WITH RESULTS OF REF. 3 AND SYSTEM III FOR DIFFERENT PRESSURES

$T_{initial} = 1667^{\circ}K$ $\varphi = 1$

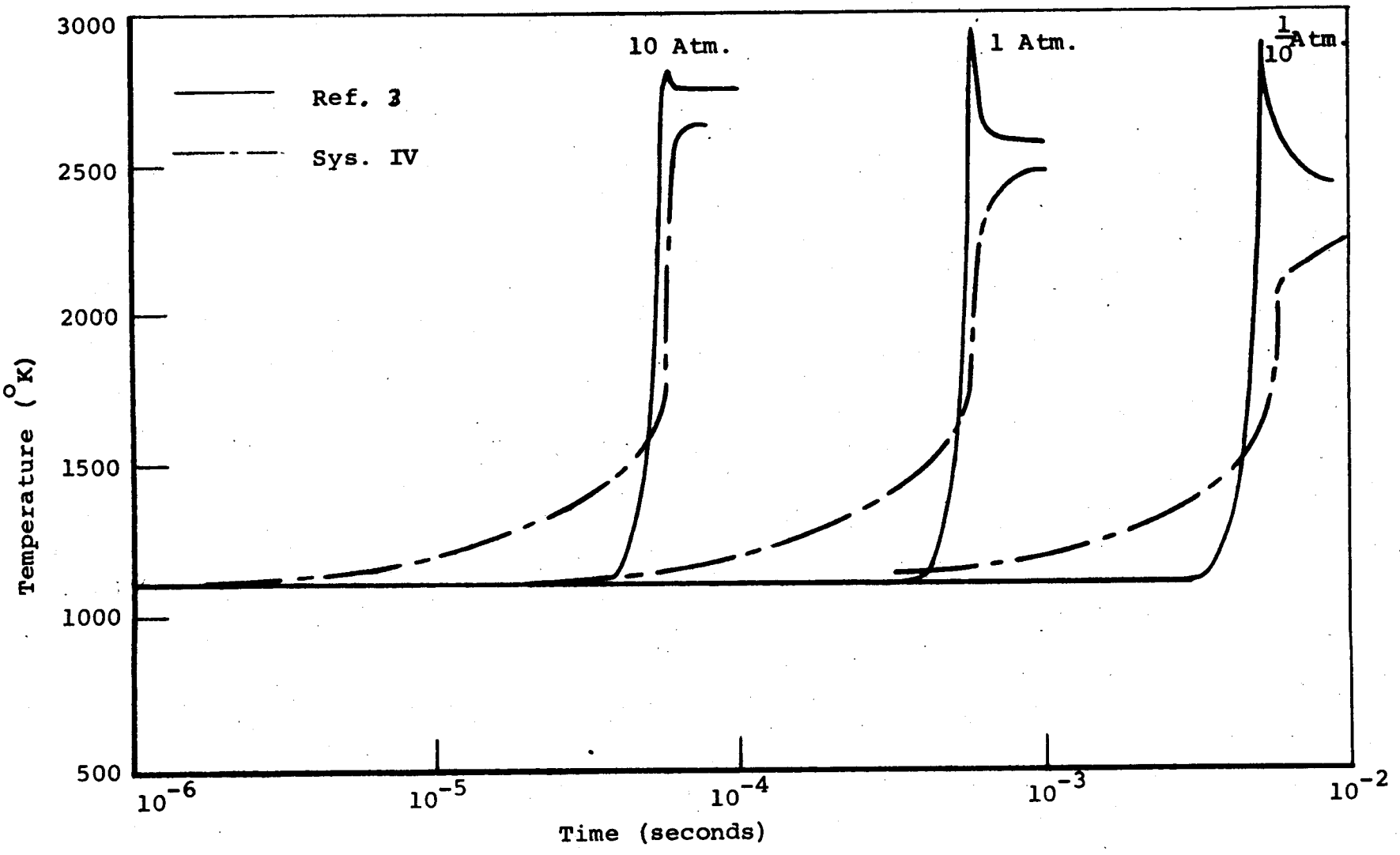

FIGURE 11 - COMPARISON OF QUASI-GLOBAL MODEL (SYSTEM IV) WITH DETAILED CHEMICAL KINETIC MODEL OF REFERENCE 3

$T_{initial} = 1111^{\circ}K \qquad \varphi = 1$

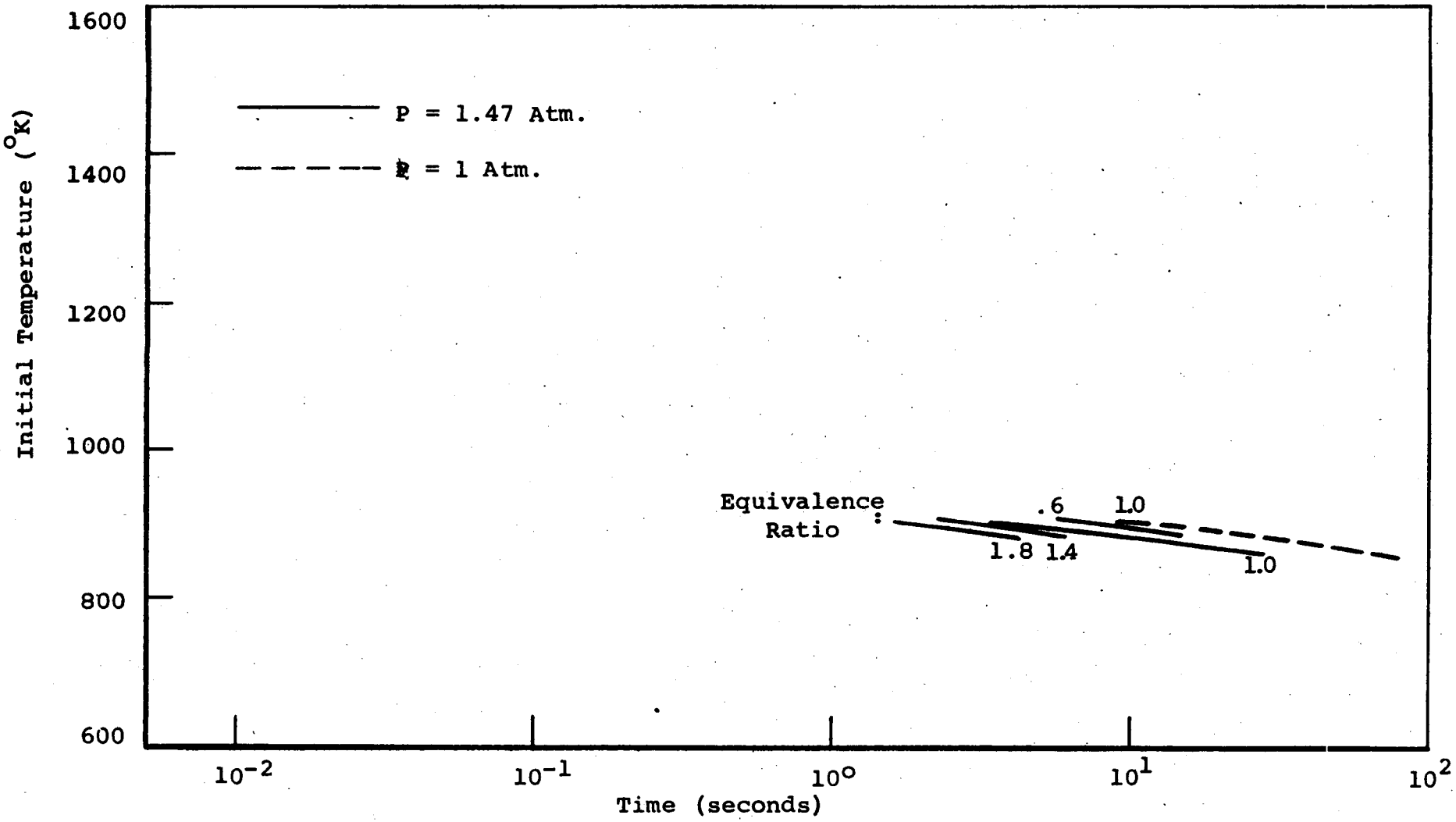

FIGURE 12 - IGNITION DELAY TIME RESULTS OF BURWELL AND OLSON (REF. 24) FOR A STEADY FLOW ISOCTANE-AIR

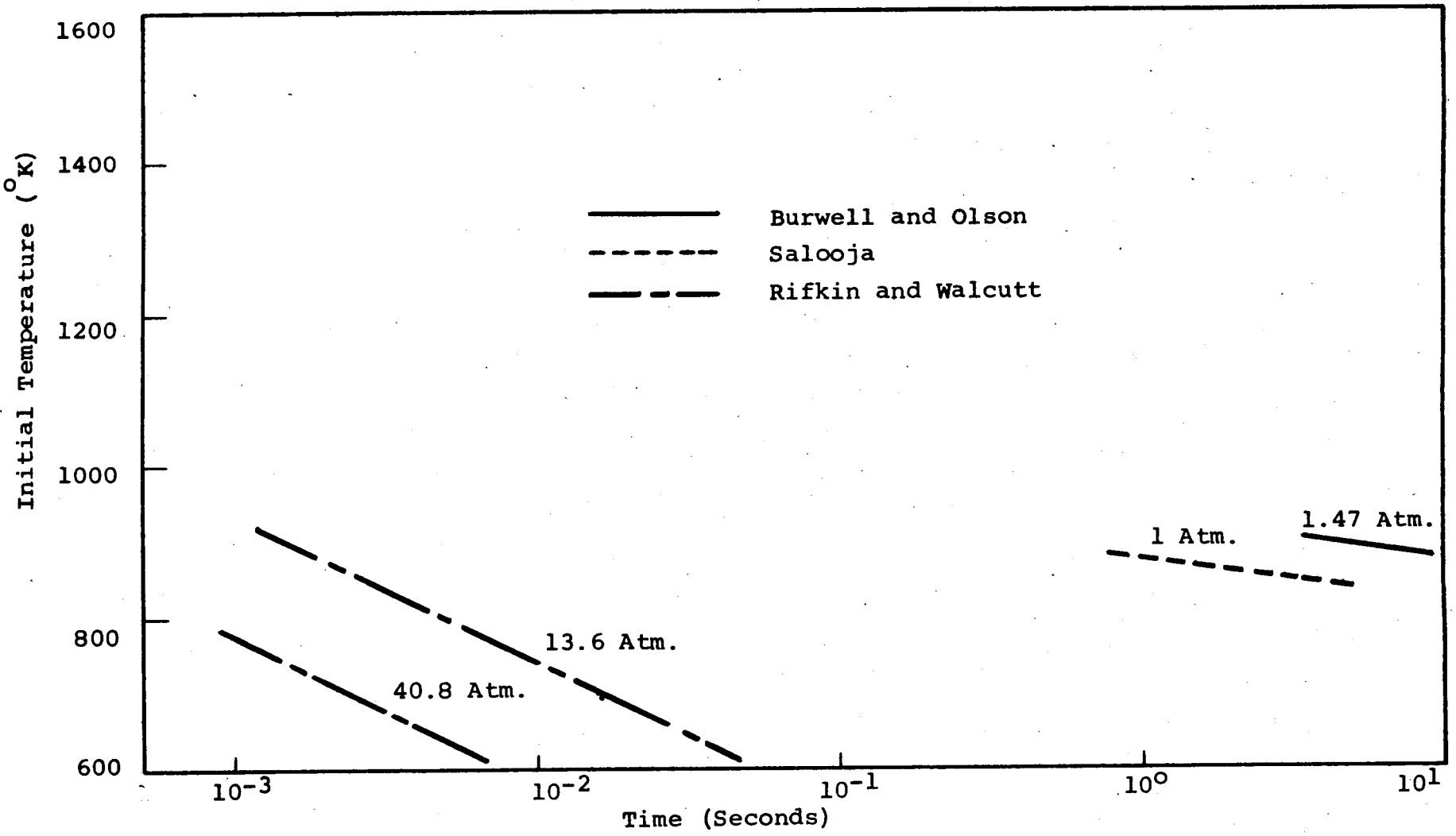

FIGURE 13 - COMPARISON OF IGNITION DELAY TIME RESULTS FOR STOICHIOMETRIC ISOOCTANE-AIR STEADY FLOW SYSTEMS

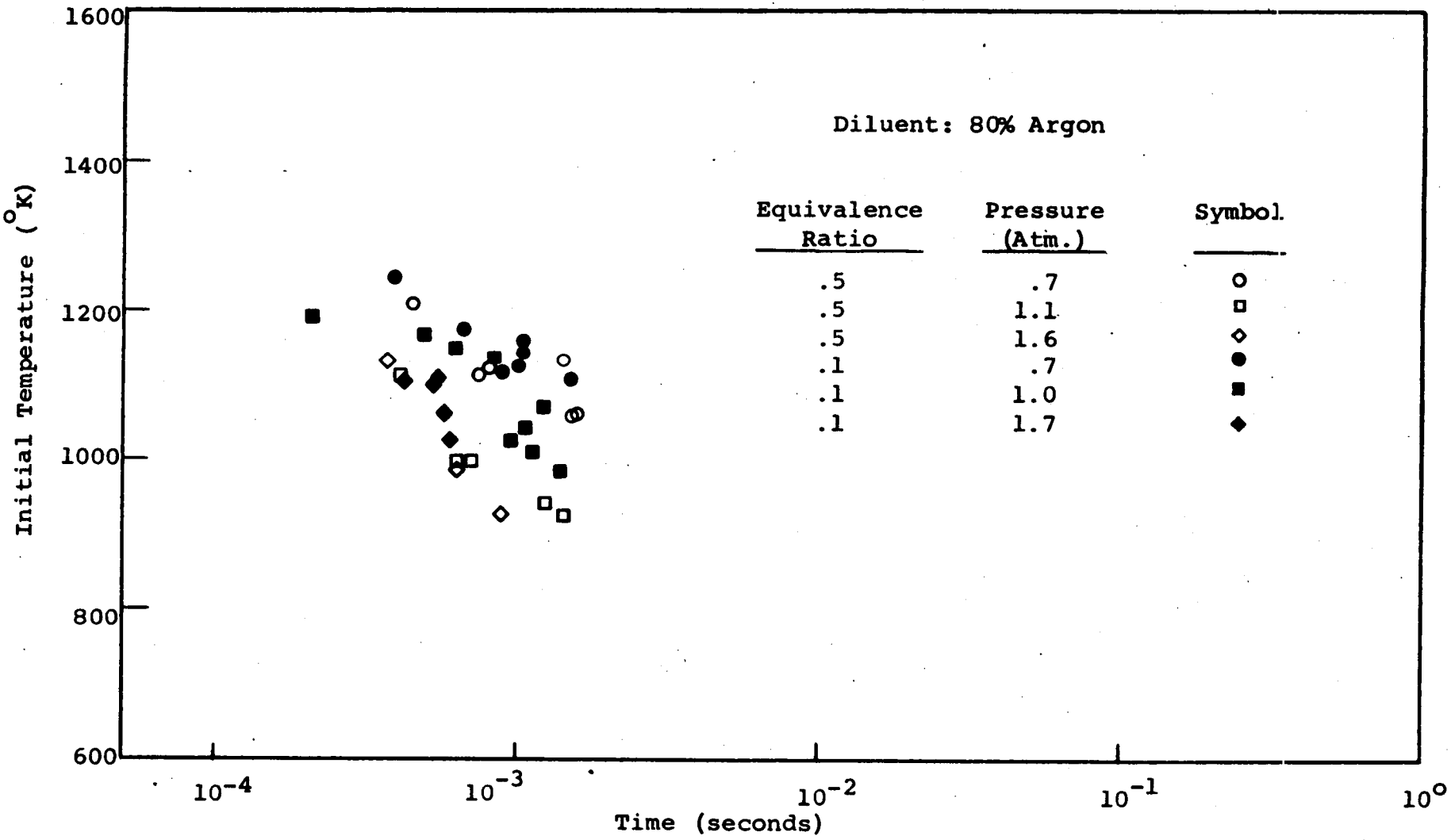

FIGURE 14 - SHELL SHOCK TUBE IGNITION DELAY STUDIES FOR PROPANE-OXYGEN ARGON MIXTURES (REF. 23)

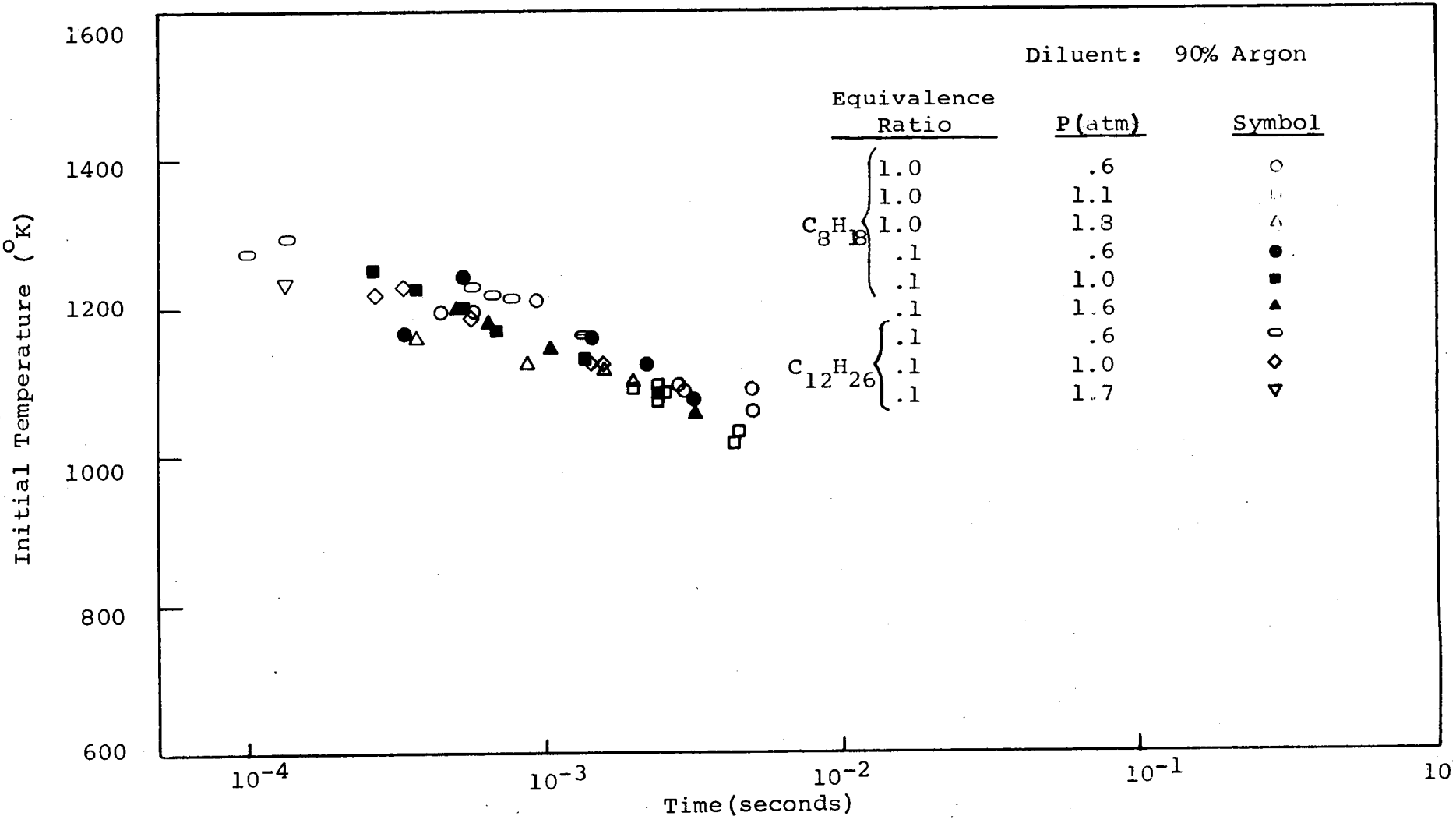

FIGURE 15 - SHELL SHOCK TUBE IGNITION DELAY STUDIES FOR n-OCTANE-ARGON AND n-DODECANE-OXYGEN-ARGON MIXTURES (REF. 23)

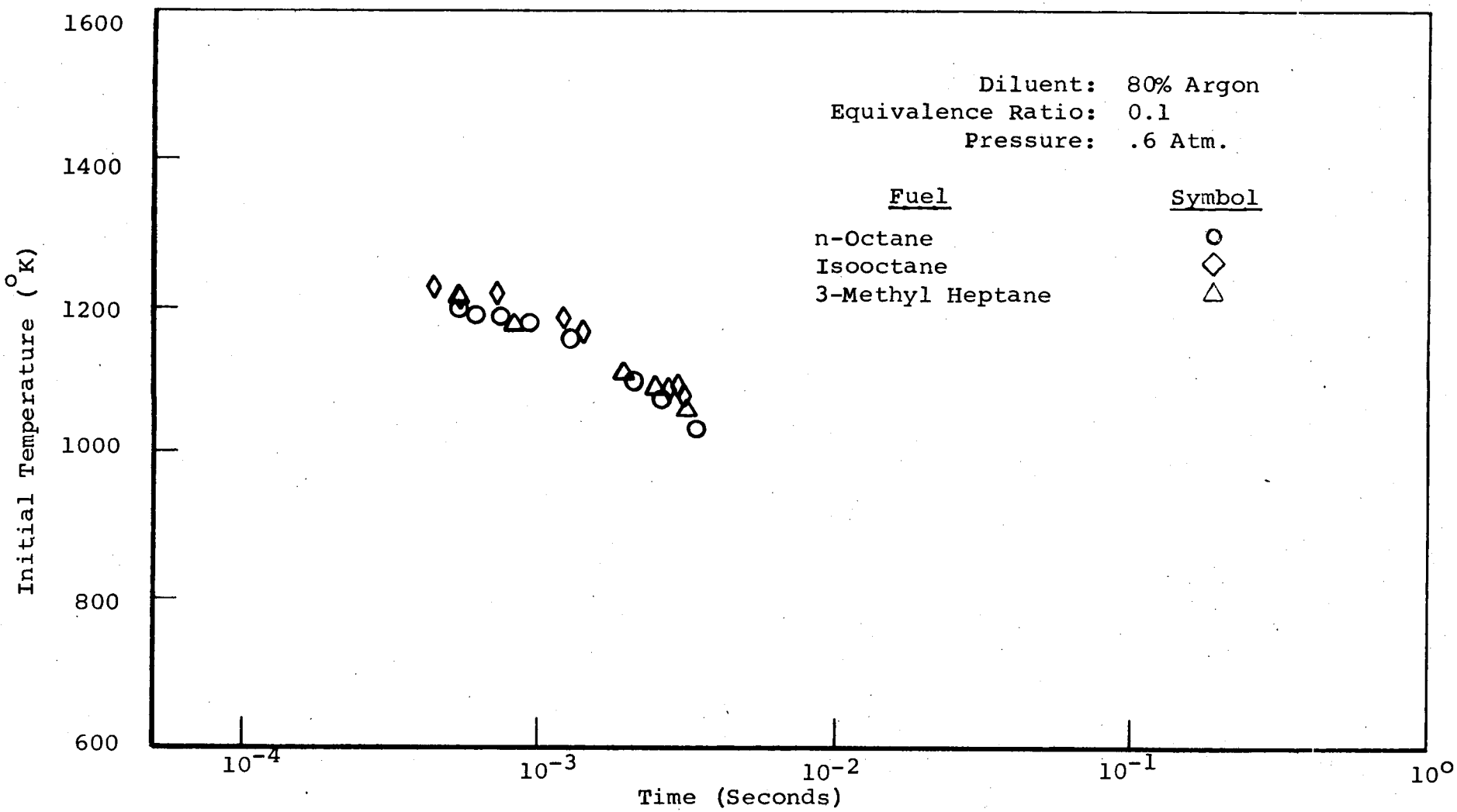

FIGURE 16 - SHELL SHOCK TUBE IGNITION DELAY STUDIES FOR DIFFERENT FORMS OF OCTANE AND HEPTANE

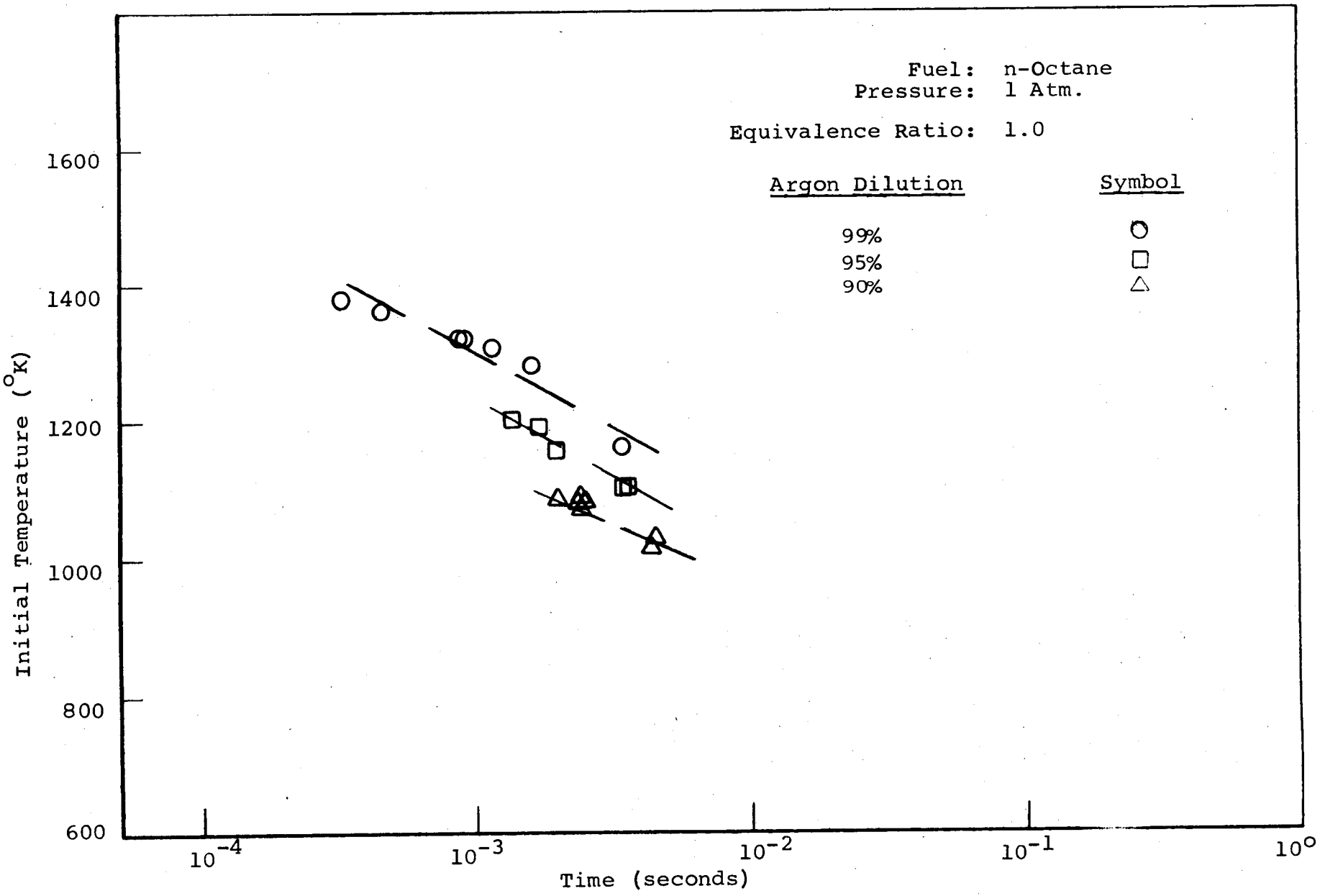

FIGURE 17 - EFFECT OF INCREASING ARGON DILUTION IN SHELL SHOCK TUBE STUDIES (REF. 23)

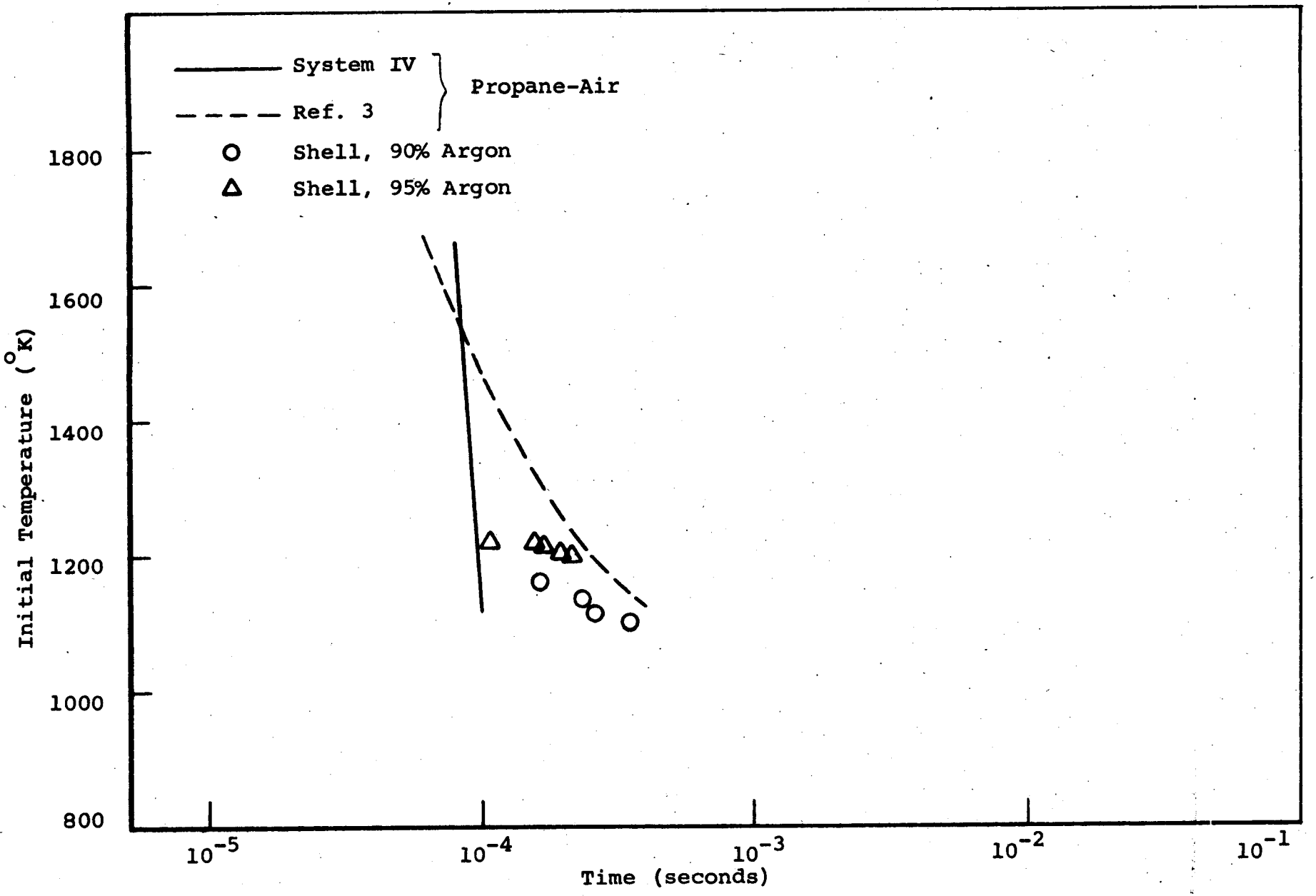

FIGURE 18 - COMPARISON OF SHELL IGNITION DELAY TIME SHOCK STUDIES (REF. 23) WITH THEORIES OF CHINITZ AND BAURER, AND SYSTEM IV FOR STOICHIOMETRIC PROPANE MIXTURES AT ATMOSPHERIC PRESSURE

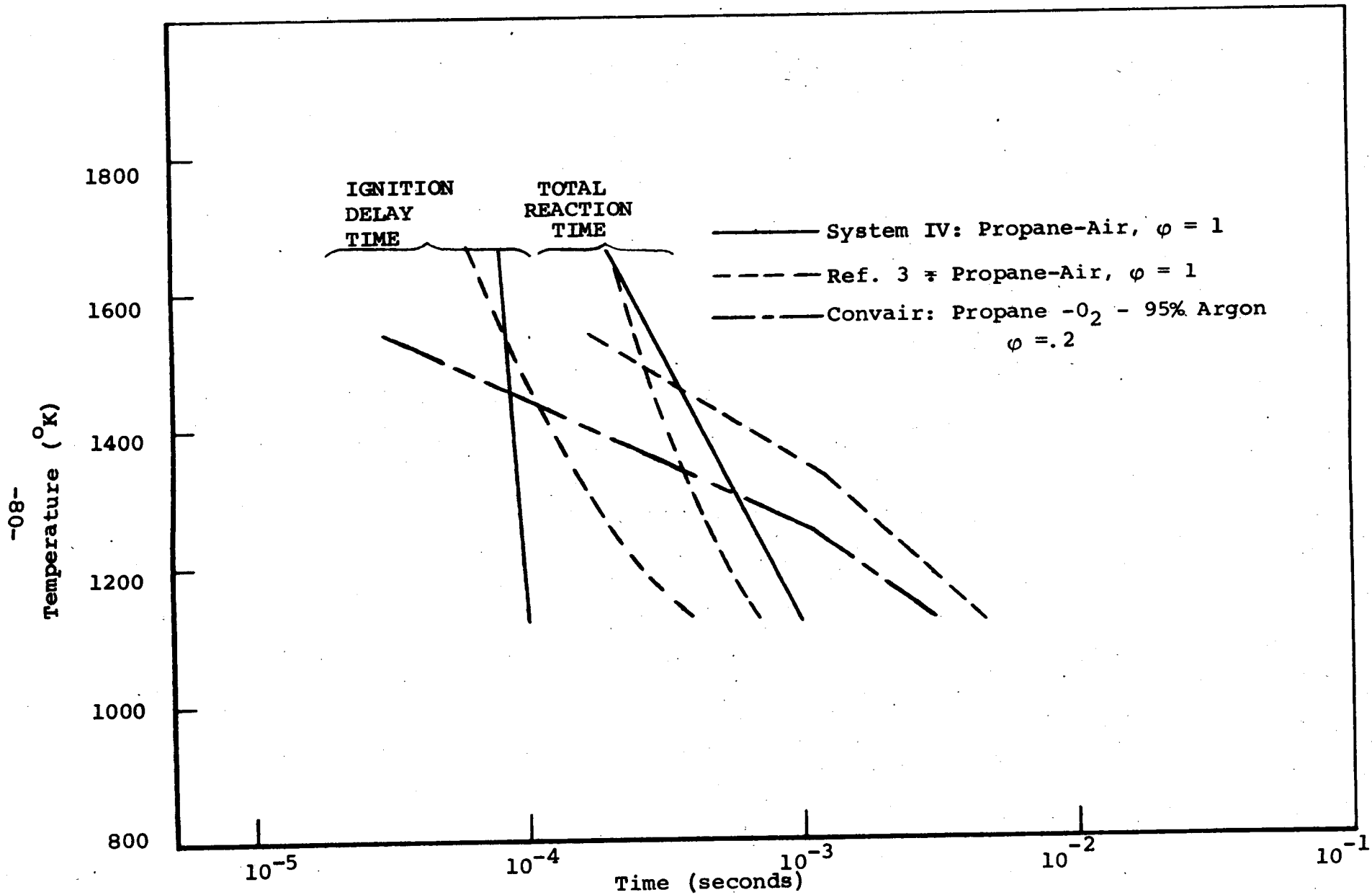

FIGURE 19 - COMPARISON OF CONVAIR SHOCK TUBE STUDIES (REF.22) WITH THEORIES OF CHINITZ AND BAURER AND SYSTEM IV FOR BOTH IGNITION DELAY AND TOTAL REACTION TIMES AT P = 1 ATMOSPHERE

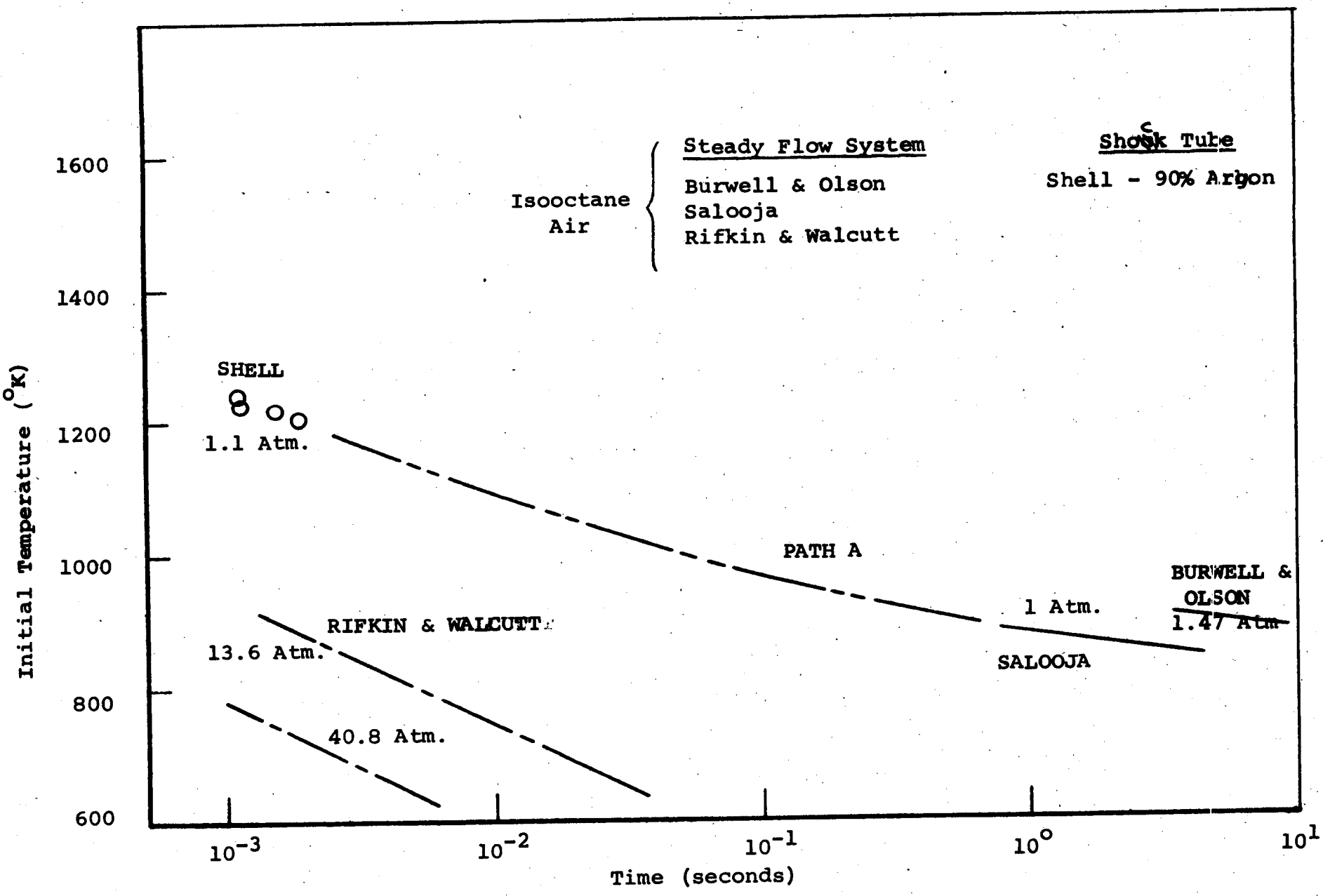

FIGURE 20 - COMPARISON OF SHOCK TUBE AND STEADY FLOW IGNITION DELAY EXPERIMENTS FOR STOICHIOMETRIC ISOOCTANE SYSTEMS

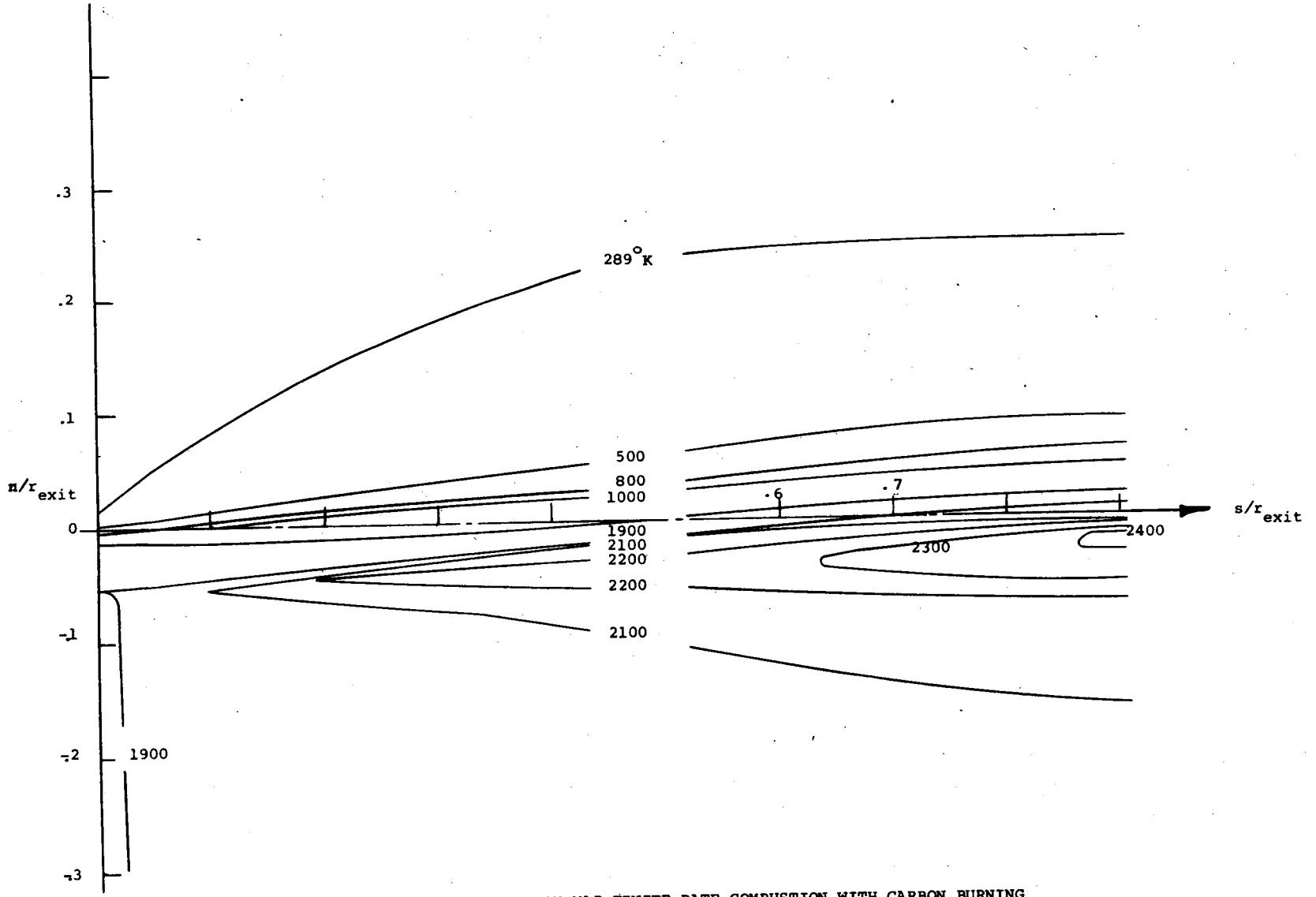

FIGURE 21 - CASE A ISOTHERM MAP FINITE RATE COMBUSTION WITH CARBON BURNING

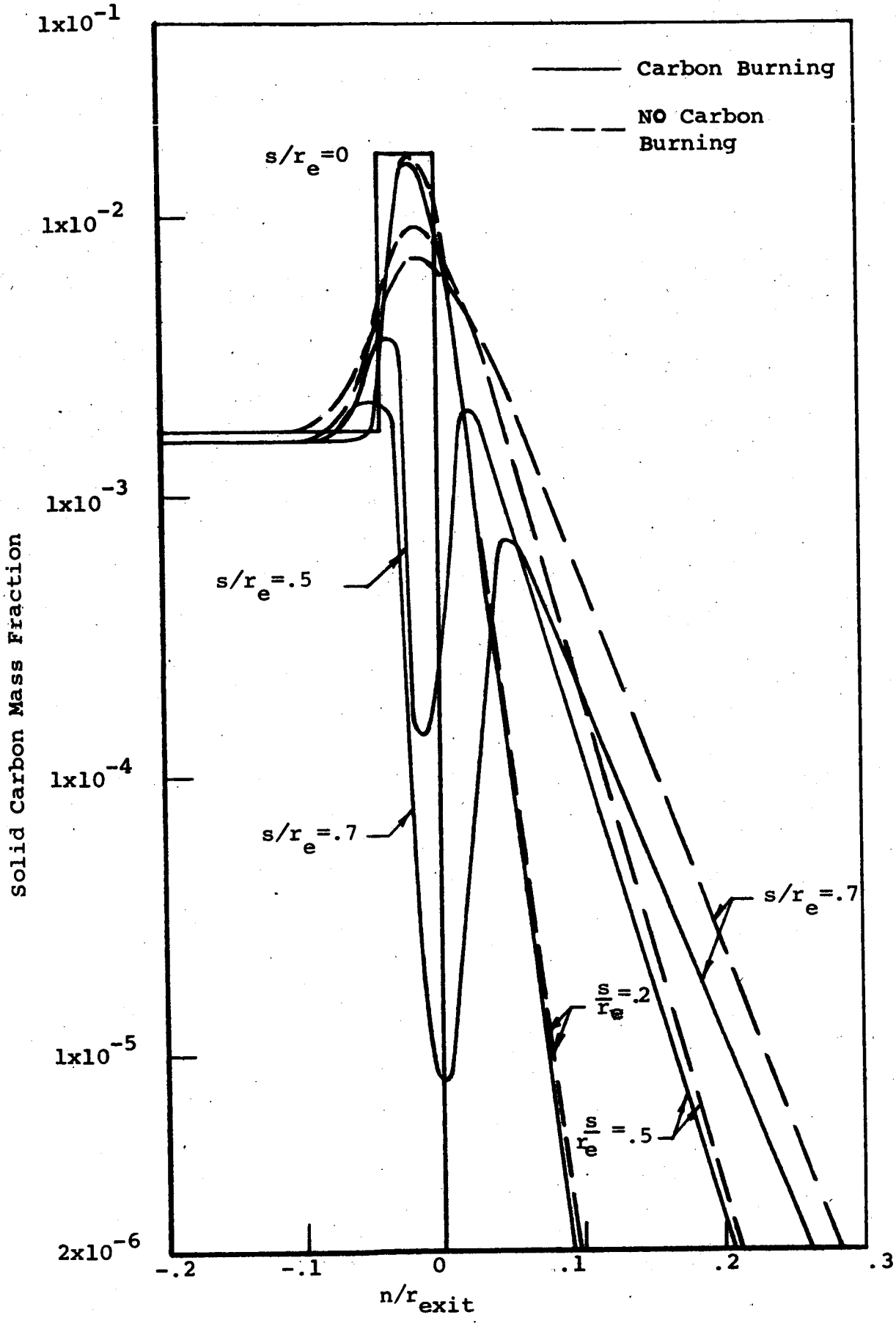

FIGURE 22 - DISTRIBUTION OF SOLID CARBON IN FLOW FIELD WITH AND WITHOUT CARBON BURNING
CASE A